Software Tools for Dynamic Cracking Analysis

Final Report

Fred W. Smith, PE
Department of Mechanical Engineering
Colorado State University
Fort Collins, Colorado

to

Joel G. Bennett
Jobie Gerken
Los Alamos National Laboratory
ESA-EA

December 21, 2000

v9

Abstract

This report deals with the ongoing development of Finite Element analysis capability for dynamic crack formation and propagation in structures. Such capability is intended for engineering analysis and design application in situations that may or may not lead to fragmentation in the structures considered. The analysis procedures discussed herein have the potential to predict the patterns of fragmentation that may occur based on tracking the growth behavior of a large number of "pre-existing" starter cracks. Discussed here are the techniques that are being called the Virtual Finite Element (VFE) approach, the Tied-Node VFE approach and the Interface Crack Element (ICE) approach.

The analyses are based on accepted approaches to the prediction of crack propagation and they make use of the currently available finite element codes ABAQUS and DYNA3D as the frameworks for analyses. Numerical results are presented for a number of test cases with the purpose of making comparisons among various numerical simulations and, in some cases, comparisons with experimental results.

Numerical results are presented for straight metal bars subjected to impact loading on both ends and on one end.

A discussion is presented on the progress toward developing practical engineering software tools to deal with the design and analysis of structures in the presence of propagating cracks under dynamic loading conditions.

Introduction

Predicting the behavior of structural components under dynamic loading conditions in the presence of propagating cracks is an area of importance and one in which the need for development of analysis and design tools continues. Important areas in this regard include rapid deformation of components caused by High Explosive (HE) detonation, spalling of components, ignition/reaction spread via propagation of cracks in High Explosive materials and high deformation rate forming processes in manufacturing.

There is a need for an "engineering" Finite Element (FE) approach to predicting crack initiation and propagation, one that can be applied with levels of effort consistent with typical engineering best practices. This means that the code applications developed must have a suitable degree of robustness and be readily available to practicing engineers in environments in which they can be easily applied. In addition, there is the need to have the FE model include dynamic effects, nonlinear material behaviors and nonlinear kinematics. The FE model should predict initiation of pre-existing cracks that will grow and coalesce as a failure initiates and proceeds and the FE model should predict crack paths rather than have crack paths predetermined.

The implementation of these developments must be ***verified*** such that the results have the highest reasonable fidelity to the physics and to the numerical approaches involved in the processes. Such verification is undertaken by assuring that the FE results compare well

with accepted analytical and theoretical results or with trusted numerical results on relevant examples. It is also necessary that these developments be ***validated*** such that the results have been confirmed to compare well with experimental results for situations that are relevant to real problems. Validation can occur by analyzing experiments for which results are available and with which comparisons can be made with the numerical predictions. In undertaking such comparison, it may be necessary to cooperate with experimentalists to assure that the experiments and measurements are useful and appropriate for comparisons with the numerical results.

In some applications there has been a practice of "killing" finite elements within a mesh as a way to model local failures. In the "killing" approach, an element is removed from the mesh and from further interaction in an analysis at some point in time. In dynamic analyses, this approach may lead to discarding mass, momentum and kinetic energy in cases where realistically the discarding of these quantities is incorrect. Further, such approaches may lead to nodal points in the FE mesh flying away from the rest of the mesh in unrealistic and incorrect ways, thus not modeling a problem with the degree of fidelity desired.

Background

The Engineering Analysis group of the Engineering sciences and Applications division (ESA-EA) of the Los Alamos National Laboratory commonly works with the Finite Element packages ABAQUS standard, ABAQUS explicit and DYNA3D among others. These packages have dynamic capability as well as capability to handle nonlinear material behavior and nonlinear kinematics. However, in the work being discussed here, there is a need to model the presence of pre-existing cracks and to allow them to propagate.

To do that, the approach taken here is to prepare multi-noded meshes and to place the "virtual" cracks at every element interface in the mesh. As a dynamic analysis progresses, the fracture mechanics analysis of the crack at each interface is conducted and the growth of the crack is predicted based on defined local fracture properties at the interface. When the interface crack grows to sufficient size, the conditions that hold the interface together are relaxed. In this way, the formation of a macroscopic crack at that interface is simulated. Such interface cracking can occur at any element interface location in the mesh so that multiple interfaces can fail and coalesce into larger macroscopic cracks. When these processes are modeled in a dynamic finite element code, the wave propagation effects are modeled in the mesh as they are affected by the propagation of the cracks within the mesh. The process is very much influenced by the local fracture behavior properties that are prescribed at the interfaces.

With some work, packages such as ABAQUS and DYNA3D are able to accommodate analysis conditions such as these, but it is necessary to develop methods to address local crack behavior and interface separation conditions, and implement special elements in some cases, that will operate in the context of these programs. Discussion of how these matters are addressed is contained in the balance of this report.

Investigation into interface cracking simulation indicates that possibly the first development, Li and Reed (1)*, is the work of Goodman *et al* (2). In this work, the authors developed a special, zero thickness, interface finite element to model the quasi-static behavior of joints and seams in rock. The method simulates the propagation of cracks in an interface element by reducing the interface element stiffness to zero after a normal-stress fracture criterion has been exceeded. Applications of finite element analysis using multi-noded meshes date back to the early 1980's with the work of Kanninen *et al* (3). Also, Liaw, *et al,* (4) used a double noding technique in which analyses were conducted to determine dynamic stress intensity factors for cracks running along pre-determined paths at prescribed velocities based on the J integral fracture criterion.

More recently, Needleman, *et al,* have developed a discrete dynamic crack propagation model for micro cracks in which continuum finite elements are bonded together by interfacial cohesion forces, (5), (6), (7), (8). The analyses are based upon an assumed relationship between the traction and displacement jump between element nodes at the interface between elements to characterize the interfacial cohesive forces. Results have been presented for material models representing isotropic-hyperelastic (9), elastic-plastic (7), and elastic-viscoplastic behaviors, (10 - 12). This method has proven effective in a number of different applications. Siegmund, *et al,* have used the technique to model the dynamic propagation of a crack across an interface (e.g. a crack originating in an iron carbide particle propagating into the surrounding ferrite), (11).

Camacho and Ortiz have incorporated this interfacial cohesion model with a damage model to model impact damage of brittle materials, (13), while Xu *et al*, (14), have investigated the effects of inhomogeneous toughness on dynamic crack growth. Difficulties arise when applying the method to dimensions typical of engineering structures because the applications have typically been applied to structures the size of 10 mm or less with the size of the elements being much smaller. Engineering structures can have dimensions that are many times larger than the structures that have been analyzed thus far with this method.

In a method identified as the Discrete Particle Computer Simulation (DPCS), Potapov and co-workers have developed an approach by which to analyze either rigid or deformable solids that are made up of particles bonded together by cohesive interfaces, (15), (16), (17). In this approach, the interface bonds are allowed to break at a predetermined maximum tensile stress and new crack surface is thus formed, thereby simulating discrete fracture.

The particles involved are treated in three different ways, but for all cases, the interface model is the same. In the first treatment, the particles are taken to be rigid two-dimensional elements so that the overall behavior is dominated by the interface properties. In the second treatment, the particles are modeled as deformable two-

* Numbers in parentheses refer to references listed in the reference section of this document.

dimensional elements. In this case, the overall behavior is dominated by a combination of the interface properties and the particle properties. In the third treatment, the first treatment was repeated in three dimensions, that is, three-dimensional rigid particles bonded together by deformable cohesive interfaces.

In each case, the portion of the model that is of interest, with regard to discrete fracture modeling, is the cohesive interface. The interface is modeled as a continuous distribution of material that is modeled as elastic, elastic-plastic, viscous, or with other behaviors. As the body deforms, resistive normal and tangential tractions are created at the solid interfaces. If the normal traction at any point along the interface exceeds a predefined limit stress, the normal component of traction is made to vanish at that location. Further, a complex algorithm is developed to handle the interference of interfaces before and after separation occurs. Newton's Second Law is enforced within each particle rather than by assembling the global stiffness and mass matrices and solving the equation for the whole system so this approach may be more similar to an explicit finite element approach than it is to am implicit finite element approach. Several examples were presented that appeared to represent reasonably well the qualitative features of expected results.

In a technique called the Element Free Galerkin (EFG) method, Belytschko and others have recently been developing a technique to model dynamic fracture, (18 – 22). It is suggested that the EFG might be an improvement on other computational methods in fracture because of the ease of creation of new surfaces. A continuum is constructed of a set of nodal points that are contained within the given geometrical description. Moving least square interpolants, in which a list of nearest neighbors must be known, are then used for the trial and test functions used in the Galerkin method.

A crack is modeled by introduction of its surface into the geometrical description of the body. The method has shown some improvements, and deficiencies, when compared to the finite element method. It has shown some promise in the modeling of dynamic fracture and is still in the development stage.

The method implemented thus far in EFG can seek the direction of crack propagation in that the crack is defined to grow at a constant velocity perpendicular to the maximum hoop stress. Using the equations of dynamic LEFM, the hoop stress is calculated as a function of angle around the crack tip and the crack is assumed to grow in the direction of maximum hoop stress at a constant speed. Although this method is still in relative infancy, the results presented by the authors for both static and dynamic fracture modeling are shown to agree well with known solutions. Some problems in the EFG method are also pointed out and new methods are being developed to address these problems. Enriched methods, (23), have been developed by which a singularity corresponding to elastostatic fracture has been incorporated into the formulation. Also, EFG has been coupled with FEM, (20), so that the beneficial aspects of EFG can be incorporated at specific locations in the structure while finite elements can be used elsewhere to take advantage of their ease of use in structural modeling.

Many of the techniques summarized in this section have been shown capable of modeling discrete crack growth, for specific problems, along paths that are not predetermined. Although each of these techniques could be applied to a wide range of problems, difficulty arises when the techniques are applied to engineering scale problems. The methods become either very computationally expensive or simply cumbersome to apply. With the exception of the DPCS and EFG methods, the techniques have not been applied to structures of engineering scale at all.

The VFE concept

The technique that has been dubbed the Virtual Finite Element (VFE) method is an adaptation of an interface element that has specific behaviors ascribed to it. It has been incorporated into the explicit FE code DYNA3D, and, as developed to date, is applicable to two-dimensional and three-dimensional analyses. As an example to demonstrate the approach, Figure 100 shows a rectangular two-dimensional body containing what appears to be an ordinary two-dimensional finite element mesh. However, this mesh is multi-noded and has four finite element nodes at each of the internal corners and two nodes along the edges of the rectangular body. For purposes of illustration, four elements are identified in Figure 100 as A, B, C and D.

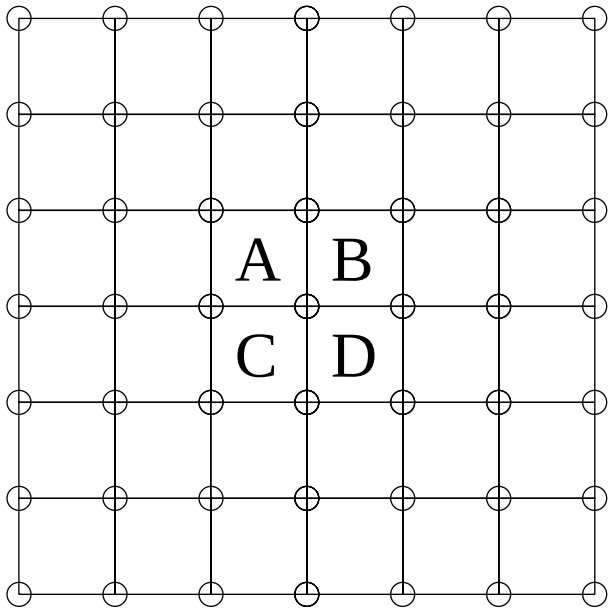

Figure 100. Multi-noded Two Dimensional Mesh

Figure 101 shows these elements in a separated view to indicate the presence of the four nodes at the corner common to the four elements. In this figure, the four nodes are shown, for clarity, as being separated, but they are in the same initial location at the beginning of an analysis. This definition allows for interfaces to be continuous or to be separated. When they separate, they simulate the fracture process.

The VFE concept assumes that there is a "virtual" interface element present between the pairs of elements shown in Figure 101. These virtual elements serve to hold the

neighboring elements together under the application of load and they have several special properties ascribed to them. Most importantly, every one of these elements has a small "starter" crack present in it. The starter cracks are thought of as representing a coalescence of microscopic material defects that are present in engineering materials and they serve as the starting point of crack propagation between the finite elements. In this way, cracks that initiate from these starter cracks may grow along the borders of the finite elements and such cracks may coalesce and develop along paths that are not pre-determined except that the paths must follow the element edges. The crack paths that develop are controlled by the mechanics of the problem as simulated by the finite element code and by the fracture behavior of the interface cracks.

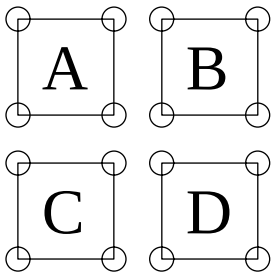

Figure 101. Four Neighboring Elements

The VFE's have several other properties ascribed to them. Among these is the assumption that the VFE has no mass. In this way all the inertia and kinetic energy of the problem being analyzed is contained within the "regular" finite elements and failure and separation that occurs in the virtual elements does not affect the analysis by artificially discarding kinetic energy. The VFE's do serve as a sink for that energy required to drive the cracking process. This approach avoids the kinds of problems of improper tracking of the kinetic energy that can occur when element "killing" is done. Further, the VFE can be treated as though it were in static equilibrium at all times, even in a dynamic problem because there is no mass ascribed to it. The behavior of the VFE's also adds compliance to the structure before crack propagation initiates as well as afterward which provides a realistic model of how the material might behave in the presence of the postulated starter defects.

A conceptual diagram of the interface element is shown in Figure 102(a). This figure shows a VFE residing between the two "regular" elements A and C from Figures 100 and 101. The VFE is drawn in solid lines while the neighboring "regular" elements, A and C, are drawn in dotted lines. The nodes for the regular elements are shown as open circles and the virtual nodes for the VFE are shown as solid circles. These nodes are numbered 1 through 4. The VFE is taken to have a width that matches the width of elements A and C, and it is taken to have a small but finite height. Figure 102(b) isolates the VFE and shows the coordinate system and the dimensions of the VFE. It is assumed that the corner nodes of the VFE have the same displacements as the corresponding corner nodes of the regular elements. For example, nodes 1 and 2 on element C have the same displacements as nodes 1 and 2 on the VFE respectively. The same is true for

nodes 3 and 4. The following sections discuss the development of the theory for implementation of the VFE in the DYNA3D code.

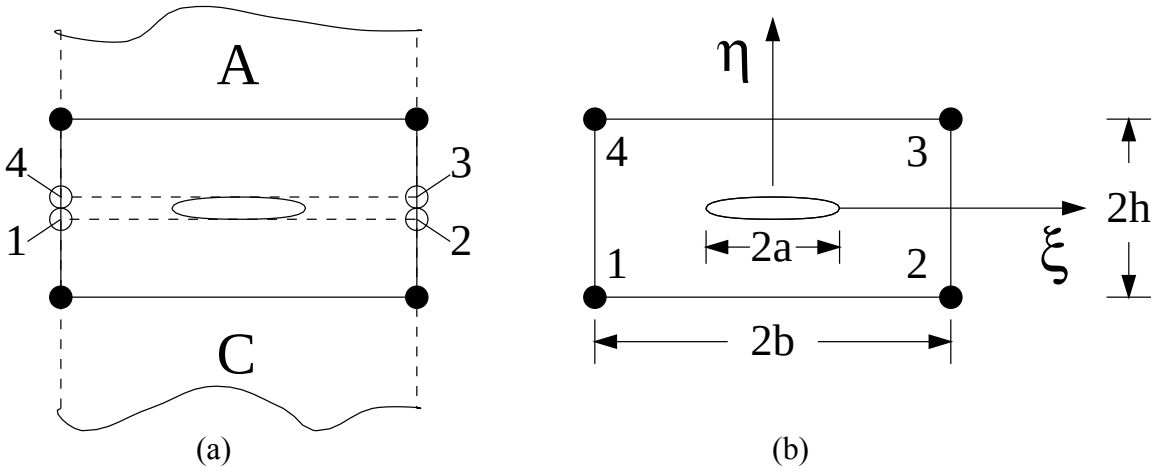

Figure 102. (a) VFE Shown Between Two Neighboring Elements A and C; (b) The VFE with Coordinate Axes and Dimensions.

DYNA3D is an explicit finite element code. The implementation approach taken was to expect the code to provide the displacements at each node in the mesh at the end of a time step. Then, given the values of the nodal displacements, a consistent set of remote shear and normal stress components in the neighborhood of the VFE can be calculated based upon the equations of static elasticity describing the crack in the VFE. These remote stresses are identified in Figure 103 and are designated σ_0, σ_1, and τ_0. Knowing these stresses, the local elastic field equations for the crack are used to approximate the behavior in the VFE. These equations are used to compute the mean stresses along the edges of the VFE which are used in turn to calculate the nodal force contribution from the VFE. These nodal forces are then passed back to DYNA3D, which then proceeds to the next time step and the process repeats.

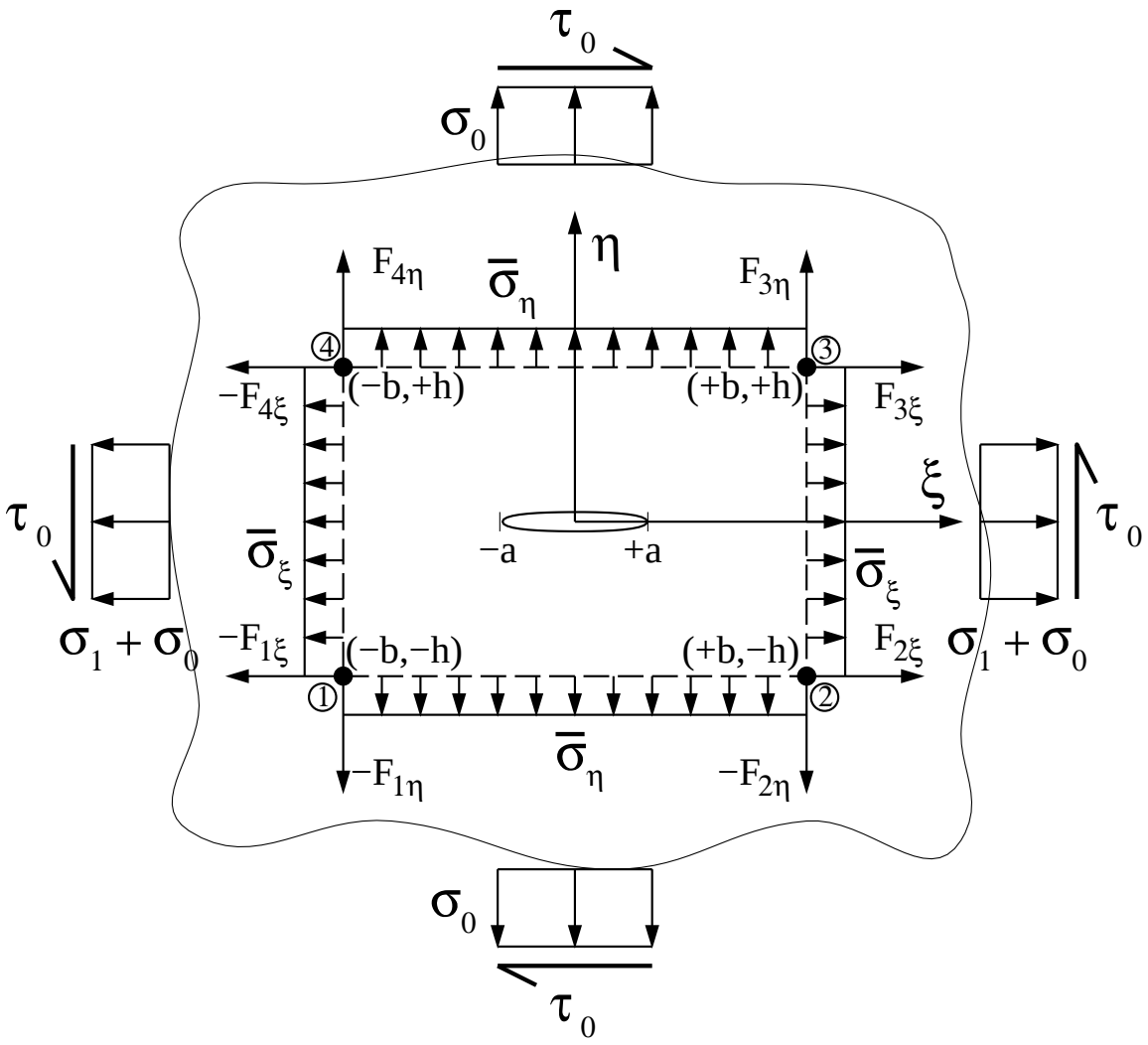

Figure 103. VFE Geometry, Stresses, Coordinates, Node Definitions and Nodal Point Forces.

The magnitude of G, the applied strain-energy-release-rate, is calculated in each VFE at each time step and is compared to the fracture toughness, G_C of the simulated material. If G is greater than G_C, the crack growth begins. Once the crack growth begins, the work flowing into the VFE is calculated at each time step and is used to compute how much the crack grows during the time step. A new crack length is calculated after each time step and once the crack length reaches the width of the neighboring elements, the VFE forces are reduced to zero and the simulation progresses from there. In this way the VFE's can simulate a growing macroscopic crack under dynamic conditions and the crack can grow in any direction as dictated by the mechanics of the simulation. Further, cracks can branch and cracks can initiate at multiple locations in the mesh at the same time and can grow as multiple cracks as well.

The VFE Formulation

In order to determine the nodal forces for each VFE, their behavior is approximated by Linear Elastic Fracture Mechanics (LEFM). The deformation field surrounding the crack in the VFE is taken to be that of a plane stress Griffith crack, subjected to uniform tension and shear remote stresses as shown in Figure 103. The Westergaard Stress Function for this case is

$$Z(z) = \frac{z}{\sqrt{z^2 - a^2}} \tag{1}$$

where

$$z = \xi + i\eta$$

For Mode I, the stress fields are given by

$$\sigma_{\xi\xi} = \sigma_0(\mathrm{Re}\, Z - \eta\, \mathrm{Im}\, Z') + \sigma_1 \tag{2}$$

$$\sigma_{\eta\eta} = \sigma_0(\mathrm{Re}\, Z + \eta\, \mathrm{Im}\, Z') \tag{3}$$

where σ_0 and σ_1 are remote stresses as shown in Figure 103. The displacements at position ξ,η are given by

$$U = U_\xi = \sigma_0\alpha_1\left[\alpha_2\, \mathrm{Re}\,\overline{Z} - \eta\, \mathrm{Im}\, Z\right] + \sigma_1 \frac{1}{E}\xi \tag{4}$$

$$V = U_\eta = \sigma_0\alpha_1\left[\alpha_3\, \mathrm{Im}\,\overline{Z} - \eta\, \mathrm{Re}\, Z\right] - \sigma_1 \frac{\nu}{E}\eta \tag{5}$$

$$\text{where} \quad \alpha_1 = \frac{1+\nu}{E}, \qquad \alpha_2 = \frac{1-\nu}{1+\nu}, \qquad \alpha_3 = \frac{2}{1+\nu} \tag{6}$$

and E is Young's Modulus and ν is Poisson's Ratio. Since Equations 4 through 6 represent the displacements in the vicinity of the VFE crack, the nodal displacements known from the code can be substituted into these equations and the equations can be solved to yield the remote stresses σ_0 and σ_1.

In order to use these results in DYNA3D, it is necessary to define the nodal displacement components as U_i and V_i, which refer to the U and V displacements at node number "i" and are related to the terms in the elastic solution through Equations 4 and 5. Now if, at the end of a time step in DYNA3D, the displacements U_i and V_i are evaluated from the code, they may be substituted into Equations 4 and 5, evaluated at the nodal locations. This sets up equations that can be solved for σ_0 and σ_1. Knowing σ_0 and σ_1 it is then possible to calculate the stresses anywhere in the neighborhood of the crack in the VFE.

In order to pass the influence of the VFE back to DYNA3D it is necessary to compute the nodal point force contribution of the VFE. This is done by first computing the average stresses along the border of the VFE by assuming those stresses will be the same as those computed from the Equations 2 and 3.

The average stress in the ξ-direction along the edge at ξ = b, Figure 103, is calculated from

$$\overline{\sigma_\xi} = \frac{1}{2h}\int_{-h}^{h} \sigma_{\xi\xi}(b,\eta)d\eta \tag{7}$$

and along the edge η = h, Figure 103, the average normal stress is

$$\overline{\sigma_\eta} = \frac{1}{2b}\int_{-b}^{b} \sigma_{\eta\eta}(\xi,h)d\xi\,. \tag{8}$$

These average stresses may be used to calculate the nodal point forces in the η-direction from

$$F_{3\eta} = F_{4\eta} = -F_{1\eta} = -F_{2\eta} = \overline{\sigma_\eta} bT \tag{9}$$

where the nodal point force components, F_{ij}, are indicated in Figure 103 and T is the thickness. Advantage has been taken of the symmetry in the Mode I solution here. Similarly the nodal point forces in the ξ-direction are calculated from

$$F_{3\xi} = -F_{4\xi} = -F_{1\xi} = F_{2\xi} = \overline{\sigma_\xi} hT \tag{10}$$

A similar development was done to include Mode II loading, but the equations are not given here since they are easily found in the fracture mechanic literature and are very similar to those already presented. Once the nodal force contributions for each of the VFE's are calculated, these forces are passed to DYNA3D and the simulation continues.

One of the practical realities that had to be addressed was that the deformation states calculated by DYNA3D do not have the homogeneity that is contained in the solutions used to represent the VFE behavior. Specifically, the VFE is not subjected to uniform tensions and shear as is assumed for the elastic solution for the VFE crack. Rather, the VFE is subjected to non-uniform tensions and shear. In order to address this situation, the following approach was taken.

First the U and V displacements of VFE node number 3 in terms of the uniform applied stresses are defined as

$$U_3^* = \sigma_0 \widetilde{U}_I(b,h) + \sigma_1 (b/E) + \tau_0 \widetilde{U}_{II}(b,h) \tag{11}$$

$$V_3^* = \sigma_0 \widetilde{V}_I(b,h) - \sigma_1 (\nu h/E) + \tau_0 \widetilde{V}_{II}(b,h)\,. \tag{12}$$

In these expressions, the terms $\widetilde{U}$ and $\widetilde{V}$ refer to the Mode I and Mode II elastic displacements for a unit applied stress calculated from the Westergard stress functions as

$$\widetilde{U}_I(\xi,\eta) = \alpha_1 \left[\alpha_2 \,\mathrm{Re}\,\overline{Z} - \eta \,\mathrm{Im}\, Z \right] \tag{13a}$$

$$\widetilde{V}_I(\xi,\eta) = \alpha_1 \left[\alpha_3 \,\mathrm{Im}\,\overline{Z} - \eta \,\mathrm{Re}\, Z \right] \tag{13b}$$

$$\widetilde{U}_{II}(\xi,\eta) = \alpha_1 \left[\alpha_3 \,\mathrm{Im}\,\overline{Z} + \eta \,\mathrm{Re}\, Z \right] \tag{13c}$$

$$\widetilde{V}_{II}(\xi,\eta) = \alpha_1 \left[-\alpha_2 \,\mathrm{Re}\,\overline{Z} - \eta \,\mathrm{Im}\, Z \right] \tag{13d}$$

The displacements of the other nodes can be determined from the symmetry and anti-symmetry conditions present in the solution from

$$U_{3I}^* = -U_{4I}^* - U_{1I}^* = U_{2I}^* \tag{14a}$$
$$V_{3I}^* = V_{4I}^* = -V_{1I}^* = -V_{2I}^* \tag{14b}$$
$$U_{3II}^* = U_{4II}^* = -U_{1II}^* = -U_{2II}^* \tag{14c}$$
$$V_{3II}^* = -V_{4II}^* = -V_{1II}^* = V_{2II}^* \tag{14d}$$

where the subscripts *I* and *II* refer to Mode I and Mode II respectively and the arabic numerals refer to the node number on the VFE.

Next we compute the average strain components for the VFE from

$$\bar{\varepsilon}_{\xi\xi} = \frac{1}{2}\left[(U_3 - U_4) + (U_2 - U_1) \right]/(2b) \tag{15a}$$

$$\bar{\varepsilon}_{\eta\eta} = \frac{1}{2}\left[(V_4 - V_1) + (V_3 - V_2) \right]/(2h) \tag{15b}$$

$$\bar{\gamma}_{\xi\eta} = \frac{1}{2}\left[(V_3 - V_4) + (V_2 - V_1) \right]/(2b) + \frac{1}{2}\left[(U_3 - U_2) + (U_4 - U_1) \right]/(2h) \tag{15c}$$

where the U_i and V_i are the nodal displacements of the VFE as calculated by DYNA. Using the symmetries and anti-symmetries in the solution, these average strains can also be expressed in terms of the U^* and V^* quantities as

$$\bar{\varepsilon}_{\xi\xi} = \frac{1}{b} U^*_{3I} \ , \quad \bar{\varepsilon}_{\eta\eta} = \frac{1}{h} V^*_{3I} \ , \quad \bar{\gamma}_{\xi\eta} = \frac{1}{b} V^*_{3II} + \frac{1}{h} U^*_{3II} \tag{16}$$

Now, using Equations 11, 12, 13, 14, 15 and 16, it is possible to set up the following equation from which σ_0 , σ_1 and τ_0 can be found

$$\begin{bmatrix} \frac{\tilde{U}_I}{b} & \frac{1}{E} & 0 \\ \frac{\tilde{V}_I}{h} & \frac{-\nu}{E} & 0 \\ 0 & 0 & \frac{\tilde{V}_{II}}{b} + \frac{\tilde{U}_{II}}{h} \end{bmatrix} \begin{Bmatrix} \sigma_0 \\ \sigma_1 \\ \tau_0 \end{Bmatrix} = \begin{Bmatrix} \bar{\varepsilon}_{\xi\xi} \\ \bar{\varepsilon}_{\eta\eta} \\ \bar{\gamma}_{\xi\eta} \end{Bmatrix} \tag{17}$$

from which

$$\tau_0 = \frac{\bar{\gamma}_{\xi\eta}}{\left(\frac{\tilde{V}_{II}}{b} + \frac{\tilde{U}_{II}}{h} \right)} \tag{18}$$

$$\sigma_0 = \frac{\bar{\varepsilon}_{\eta\eta} + \nu \bar{\varepsilon}_{\xi\xi}}{\frac{\tilde{V}_I}{h} + \frac{\nu \tilde{U}_I}{b}} \tag{19}$$

$$\sigma_1 = E\left(\bar{\varepsilon}_{\xi\xi} - \sigma_0 \tilde{U}_I / b \right) \tag{20}$$

Now, at the end of a time step in DYNA3D, these stress levels are known. It is to be emphasized that these are the uniform stress approximations required for the VFE to be in overall static equilibrium with the surrounding dynamic stress field at a given point in time.

From these stresses, it is possible to compute the standard LEFM Stress Intensity Factors for the VFE crack in each VFE in the mesh. This is done using

$$K_I = \sigma_0 \sqrt{\pi a} \tag{21}$$

$$K_{II} = \tau_0 \sqrt{\pi a} \tag{22}$$

where K refers to the stress intensity factor, *a* is the crack half-length, and the subscripts refer to Modes I and II. Next, the applied Strain-Energy-Release-Rate is computed from

$$G = \frac{K_I^2}{E} + \frac{K_{II}^2}{E} \tag{23}$$

In calculating G in this way it is assumed that the crack grows in its own plane. While in general this does not occur, it is deemed appropriate to make this approximation in this simulation approach because the cracks only grow to the extent of the width of one VFE in one plane and thereafter can change direction in accordance with the surrounding deformation field. In each VFE the crack is constrained to not grow until the condition is satisfied that

$$G \geq G_C \tag{24}$$

in which G_C is the fracture energy rate required to produce crack propagation and G is the "applied" Crack Extension Force. The next issue of importance is, once the crack starts to grow, based on Equation 24, how far will it grow during a DYNA3D time step? This issue was addressed by calculating the work going into the VFE during the time step and ascribing that work to driving the crack tip forward. The increment of work was calculated from

$$\Delta W = \sum_{n=1}^{4} \vec{F}_n \bullet \vec{V}_n \Delta t \tag{25}$$

where ΔW refers to the work increment, $\vec{F}_n$ refers to the nodal point force vectors on the VFE nodes and $\vec{V}_n$ refers to the nodal point velocity vectors on the VFE nodes. In this approach it was assumed that all of the energy going into the VFE, after cracking started, went to driving the crack tip forward. The increment of crack growth was then calculated from the energy balance

$$\Delta W = G_C(2T\Delta a)$$

or

$$\Delta a = \frac{\Delta W}{2G_C T} \tag{26}$$

for each time step and the crack size was then updated by adding Δa to the current crack size. In Equation 26, "T" is the thickness. The crack size was allowed to increase until the crack length 2*a* became equal to the element width 2*b*.

These steps constitute the original implementation of the VFE into DYNA3D. A significant amount of testing was undertaken with this implementation with some success. It was found that this approach to modeling crack initiation and propagation worked within limitations. Figure 104 shows the results of an early test simulation conducted using this approach on a center crack in a wide plate using a very crude finite element mesh. In this case, the pre-existing center-crack was placed between the two elements on the left-hand side of the mesh. All other pairs of finite elements had VFE's placed between them. The analysis was conducted with vertical tensile forces applied to all the nodes along the top and bottom. The figure shows the analysis at a point in time after the first VFE had fully failed and the macroscopic crack is propagating to the right. At the time shown the second VFE has just failed.

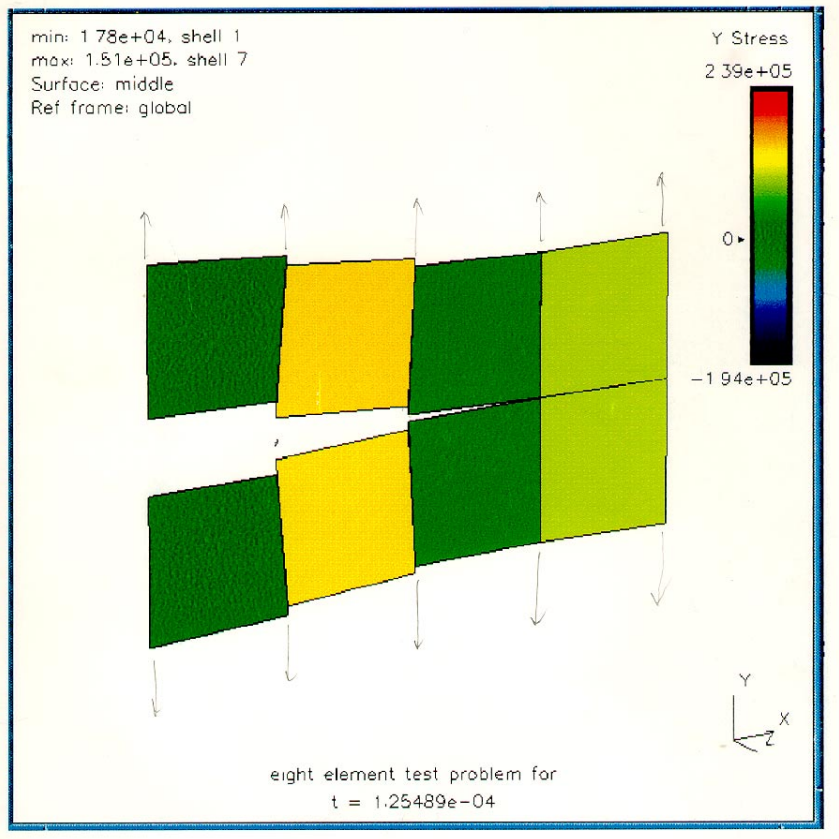

Figure 104. Eight-Element VFE Simulation of a Central Crack Loaded in Tension.

Work was undertaken to analyze problems of increasing complexity using this approach and while successes were attained, difficulties were encountered as well. One of the difficulties was that it was necessary to select "h", the element height, for each VFE. No basic reason was uncovered to select any particular height as compared to another. It was determined that if "h" was too large, the VFE's would take too much of the stress applied to the structure in the "ξ" direction, see Figure 102b, leading to an unrealistic simulation. If "h" was too small it was found that DYNA3D would be forced into a numerically unstable mode. Also, it appeared that an unrealistically large amount of shear

compliance was always present in the VFE's. The effect of this excessive shear compliance can be seen in Figure 104 to some degree. It is believed that the non-zero height of the element caused the seemingly excessive compliance in the "ξ" direction and it was probably present in the "η" direction as well, but not noticeable. To eliminate the shear compliance effects, one approach was to subtract the un-cracked elastic solution from the total solution so that only compliance due to the crack was incorporated. This improved matters, but not enough to eliminate the effect to the satisfaction of the authors.

Finally, the calculation of the work increment ΔW was done in several different ways in various attempts to resolve problems. Ultimately, the approach of calculating ΔW and using it to determine the amount of crack growth during a time step was found to not have the robust characteristic being sought and it was abandoned. It worked reasonably well for Mode I situations in which the cracks were running in a straight line and the cracks were even noted to accelerate and decelerate in response to reflected wave fronts. However, for more complicated situations, the energy flow to the VFE's did not seem to work correctly.

The change made to improve robustness, however, was a relatively simple one. Instead of calculating ΔW based upon the details of the elastic solution in the neighborhood of the VFE, an R-Curve approach was taken. In this approach the stresses σ_0 and τ_0 were computed directly from the regular DYNA3D elements neighboring a VFE. These stresses were used to compute G using Equations 21, 22 and 23 at each time step and, instead of computing the work increment, ΔW, a G R-Curve was used to determine the change in crack size.

The R-curve was taken to have the form

$$G_R = \lambda(a - a_0)^n + R_1 \tag{27}$$

The parameters λ, *n* and R_1 in this expression were determined by curve fitting to a measured, or realistically estimated, R-Curve for the simulated materials. Then, the computed G at the end of a time step was set equal to G_R in Equation 27 which was then solved for *a* to give the new crack length of a growing crack. In undertaking this approach, situations arose in which the crack growth necessary to completely separate a VFE may be larger than lengths for which "valid" R-Curve data are available. To accommodate such circumstances, Equation 27 is fitted to the part of the curve for which data exist and is used to calculate *a* until the VFE separates.

The R-Curve approach added measurably to the robustness of the VFE analysis capability, but it retains the compliance behaviors discussed earlier and still requires the selection of "h" for each VFE.

VFE Results

Figure 105 shows a sample problem that was analyzed using the VFE approach with the R-Curve. Shown in the Figure 105a is a straight bar of rectangular cross-section made from steel and subjected to a time varying uniform axial stress. The top and bottom edges and the front and rear faces of the bar are free from traction and it is idealized as being in plane stress. The bar has a width of 2.5 inches, a length of 12.5 inches, and a thickness T of 0.1 inches. The Young's Modulus and Poisson's Ratio are given in the figure as is the expression for the R-Curve
that was used.

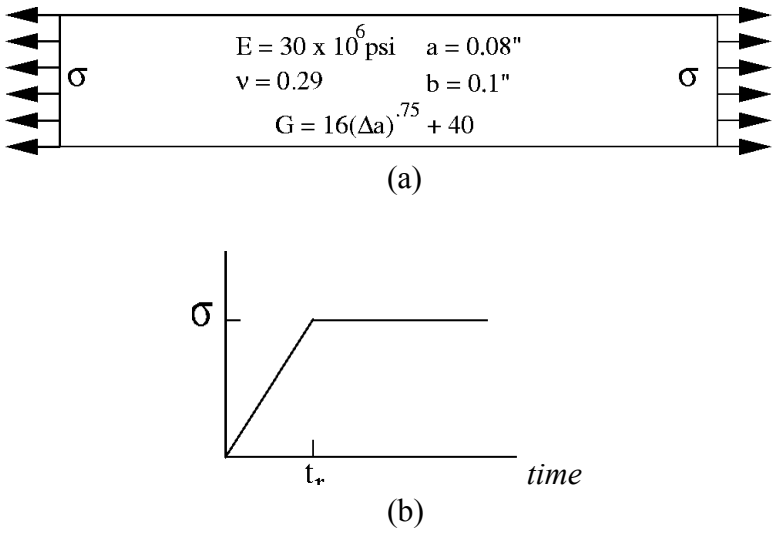

Figure 105. (a) Straight Bar Tension (sbt) Specimen; (b) Applied Loading vs time.

The parameter "a" in the figure refers to a_0 , the initial size of the cracks within each VFE

Two different loading scenarios were examined. Figure 105b which shows the applied stress increasing rapidly up to σ_{max} at time t_r and remaining constant thereafter. The two scenarios are characterized as follows:

	Maximum Stress, σ_{max}	Ramp Time, t_r
Scenario A:	35.2 ksi	1.0e-05 sec.
Scenario B:	48.0 ksi	1.0e-06 sec.

Both scenarios represent fast loading situations, but Scenario B is considerably more intense than is Scenario A.

Figure 106 shows a graph of the R-Curve used in this sample problem. This R-Curve was estimated from Fracture Toughness data given in (24) for a high strength steel with Fracture Toughness of about 35 ksi-in$^{1/2}$. It is an estimated R-Curve based on Fracture Toughness data and using

$$G_C = \frac{K_C^{\,2}}{E} \tag{28}$$

to calculate G_C. The curve fitting process was conducted by choosing the values of λ, n and R_1 as follows: First, the knee of the curve was placed close to the G_C value calculated from Equation 28. Secondly, the slope of the curve after the knee was estimated by allowing G to increase by approximately 10% while *a* doubles from a_0. This was done to provide a plausible R-Curve for these numerical tests.

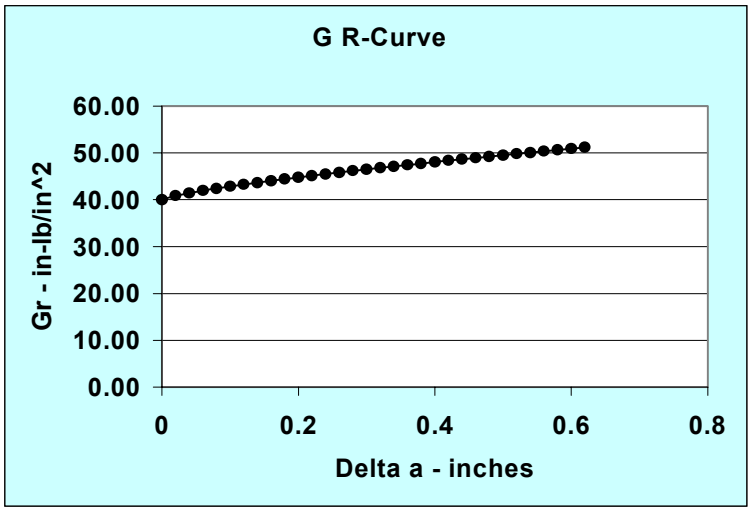

Figure 106. G R-Curve

Figure 107 shows a snapshot of the movie results from a VFE simulation for loading scenario A. In this simulation, there were only 20 regular elements as shown and there was a VFE along every internal interface between the regular elements. All of the VFE's were tracked continuously during the simulation to determine whether the initial crack increased in size and when a crack grew large enough to separate a pair of regular elements a flag was set and the time recorded when this occurred. The figure shows that the first VFE elements to "break", that is, fully separate, were numbers 15 and 14 which

are situated at the center of the bar and they broke at a time of 4.91e-05 sec and 4.94e-05sec respectively. A simple calculation shows that the longitudinal waves propagating from the ends of the bar would meet at the center of the bar and through reinforcement would reach a peak stress level at a time of about 4.1e-05 sec. From Figure 107, it is evident that, in the simulation, the bar breaks at the center as expected at about 8 microseconds after the theoretical peak stress should be attained.

The picture shown in Figure 107 is excerpted from a movie of the simulation at a time considerably later than initial failure, after the bar has broken into two pieces. The stress wave propagation prior to and subsequent to the break can be clearly seen in the movie of the simulation. That movie is presented at Hot Link 107: sbt_a_vfe_20.mov. In this movie, one can observe the wave propagation from the ends and the reinforcement of those waves when first they begin to interact at the center of the bar. One can also observe the break that occurs when the cracks grow at the center followed by the separation of the upper and lower portions of the bar. The ringing after the break can also be observed as can the lateral displacements in the elements due to the Poisson's effect as the waves move up and down the bar.

Loading Scenario A, VFE
Number of Elements: 20 element (2 x 10)
Element Dimension: 1.25” x 1.25”
File Name: /raid5/gerken/frac/rect1/paper_runs/sbt_a_vfe_20
Failures:
vfe number 15 failed, time = 4.9158441492779780E-05
vfe number 14 failed, time = 4.9481700177293480E-05

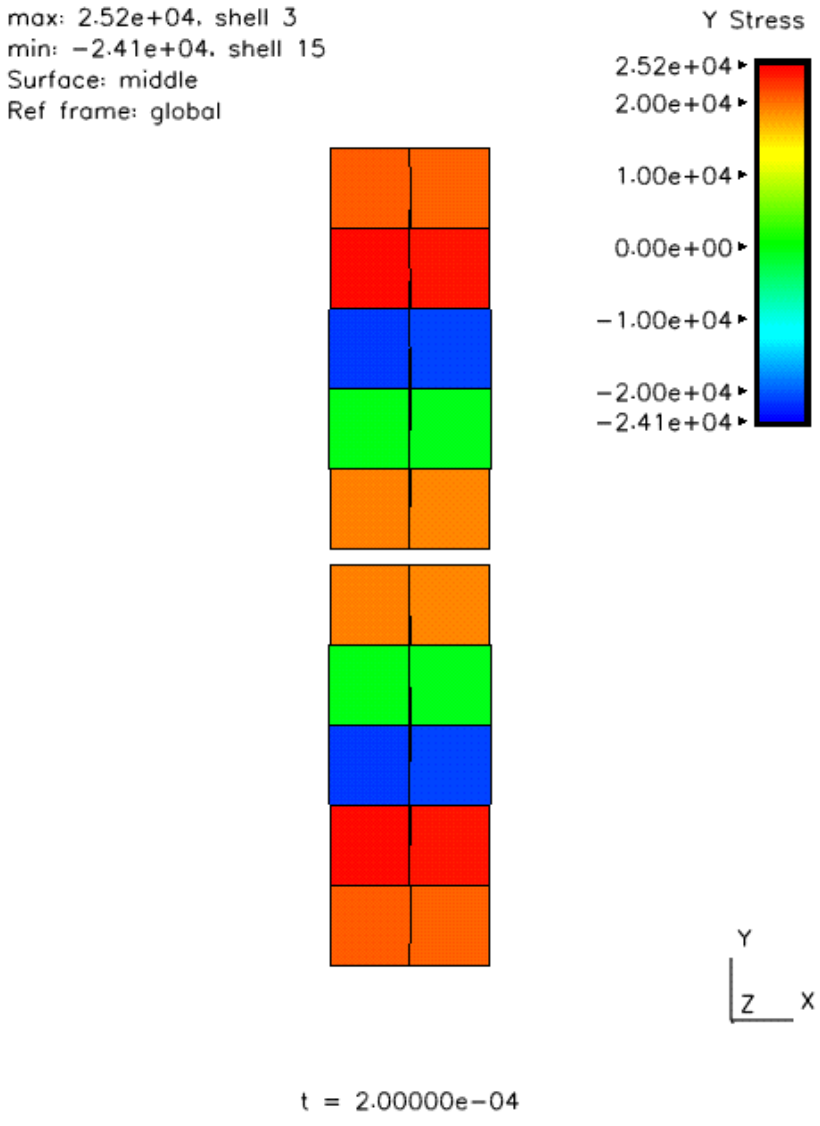

sbt_a_vfe_20

Figure 107. Straight Bar Tension, 20 Elements.

The results given in Figure 107 are for a case which has only 20 regular elements. In order to examine the effects of simulations with larger numbers of elements a number of additional cases were simulated. Figure 108 shows the same problem analyzed using 80 regular elements with VFE’s along every internal interface. This case is again loaded

with Scenario A. In this case several elements fail starting at time 4.82e-05 sec and continuing through 5.04e-05 sec at which time the central plane is fully fractured. By this time the plane one layer up and one layer down had already failed though all of this occurred within 2 microseconds. In this case, the image provided in Figure 108 is taken at the time of 1.0e-04 sec which is well past the time of these failures in the middle of the bar. The shattering effects noted may be due to the larger number of elements involved in this simulation thereby providing greater resolution than was possible in the Figure 107 problem. For example, the element dimensions in this case are one-half the size of those in Figure 107 so the increased number of interfaces allows failures to occur that could not occur in the Figure 107 case because VFE's did not exist in those locations in that case. Secondly, once a VFE fails, the subsequent simulation is affected by the presence of the open cracks that result. It is therefore reasonable to expect differences between the simulations as the number of elements increases. However, it is somewhat encouraging that the mid-plane still fails, albeit along with some shattering that occurs nearby. The simulation of Figure 108 can be observed in movie format in Hot Link 108: sbt_a_vfe_80.mov.

Number of Elements: 80 element (4 x 20) Loading Scenario A
Element Dimension: 0.625” x 0.625”
File Name: /raid5/gerken/frac/rect1/paper_runs/sbt_a_vfe_80

Failures:

vfe number	75 failed, time = 4.8293E-05	vfe number	54 failed, time = 4.9343E-05
vfe number	61 failed, time = 4.8427E-05	vfe number	60 failed, time = 4.9343E-05
vfe number	62 failed, time = 4.8751E-05	vfe number	77 failed, time = 4.9478E-05
vfe number	74 failed, time = 4.8751E-05	vfe number	53 failed, time = 4.9693E-05
vfe number	76 failed, time = 4.8885E-05	vfe number	81 failed, time = 4.9693E-05
vfe number	83 failed, time = 4.8912E-05	vfe number	67 failed, time = 4.9882E-05
vfe number	63 failed, time = 4.8966E-05	vfe number	69 failed, time = 4.9936E-05
vfe number	82 failed, time = 4.9209E-05	vfe number	70 failed, time = 4.9936E-05
vfe number	84 failed, time = 4.9289E-05	vfe number	56 failed, time = 5.0259E-05
vfe number	55 failed, time = 4.9316E-05	vfe number	68 failed, time = 5.0448E-05

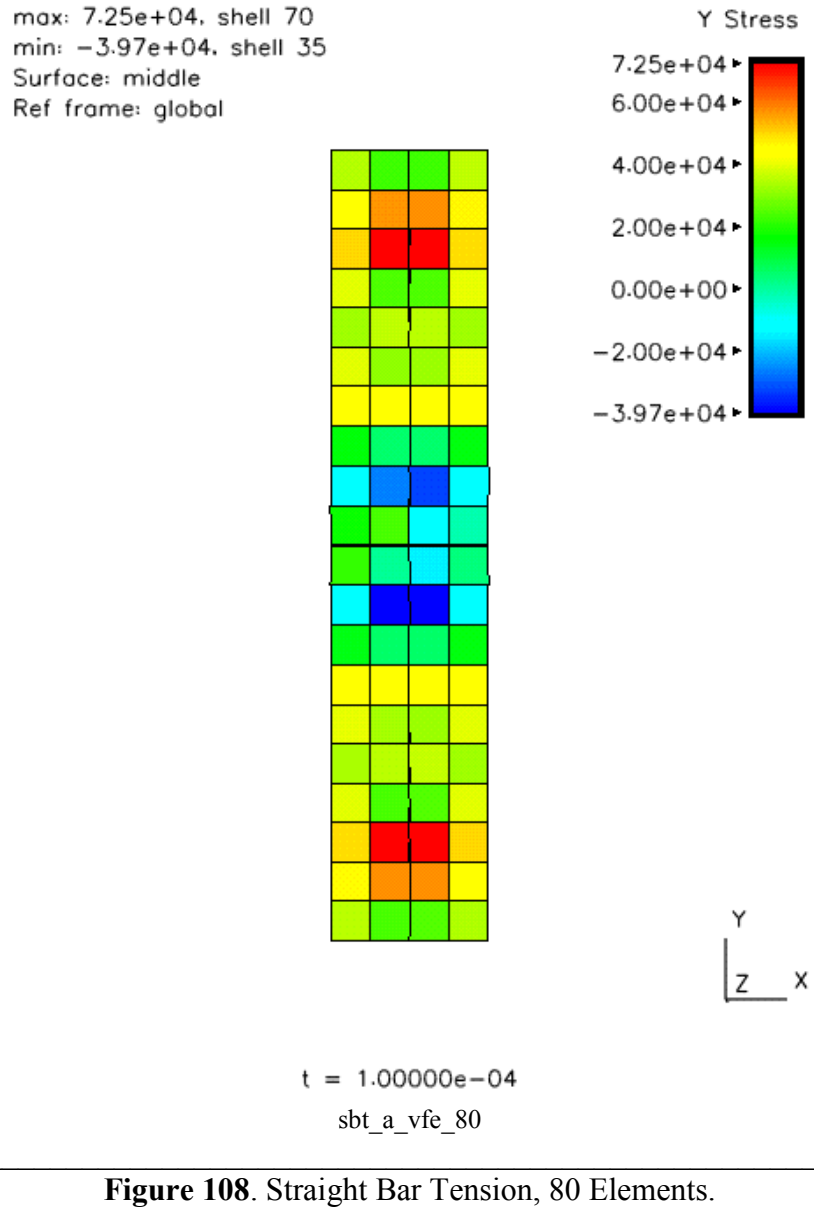

Figure 108. Straight Bar Tension, 80 Elements.

Figure 109 shows a third simulation that was conducted with even smaller elements. In this case, the elements are one-half the size of those in Figure 108. This time, the mid-plane fails first beginning at the time 4.4e-05 sec and finishing at about 4.52e-05 sec.

In the Figure 109 simulation, shattering in the mid-bar area continues after the mid-plane separates. Also, at a much later time of 1.9e-04 sec, the ends of the bar spall off. The movie format of the Figure 109 simulation can be observed at Hot Link 109: sbt_a_vfe_320.mov .

Number of Elements: 320 element (8 x 40)
Element Dimension: 0.3125” x 0.3125”
File Name: /raid5/gerken/frac/rect1/paper_runs/sbt_a_vfe_320

Failures:

vfe number 300 failed, time = 4.3995E-05
vfe number 293 failed, time = 4.4251E-05
vfe number 294 failed, time = 4.4359E-05
vfe number 299 failed, time = 4.4372E-05
vfe number 295 failed, time = 4.4844E-05
vfe number 298 failed, time = 4.4911E-05
vfe number 308 failed, time = 4.5073E-05
vfe number 296 failed, time = 4.5113E-05
vfe number 278 failed, time = 4.5127E-05
vfe number 315 failed, time = 4.5154E-05
vfe number 285 failed, time = 4.5207E-05
vfe number 297 failed, time = 4.5221E-05

shattering in center section
vfe number 311 failed, time = 6.7411E-05
vfe number 56 failed, time = 1.55675E-04
vfe number 535 failed, time = 1.5576E-04
vfe number 538 failed, time = 1.5591E-04
vfe number 57 failed, time = 1.5593E-04
end spalling
vfe number 584 failed, time = 1.9444E-04
vfe number 12 failed, time = 1.9858E-04
vfe number 579 failed, time = 1.9951E-04
vfe number 14 failed, time = 1.9957E-04

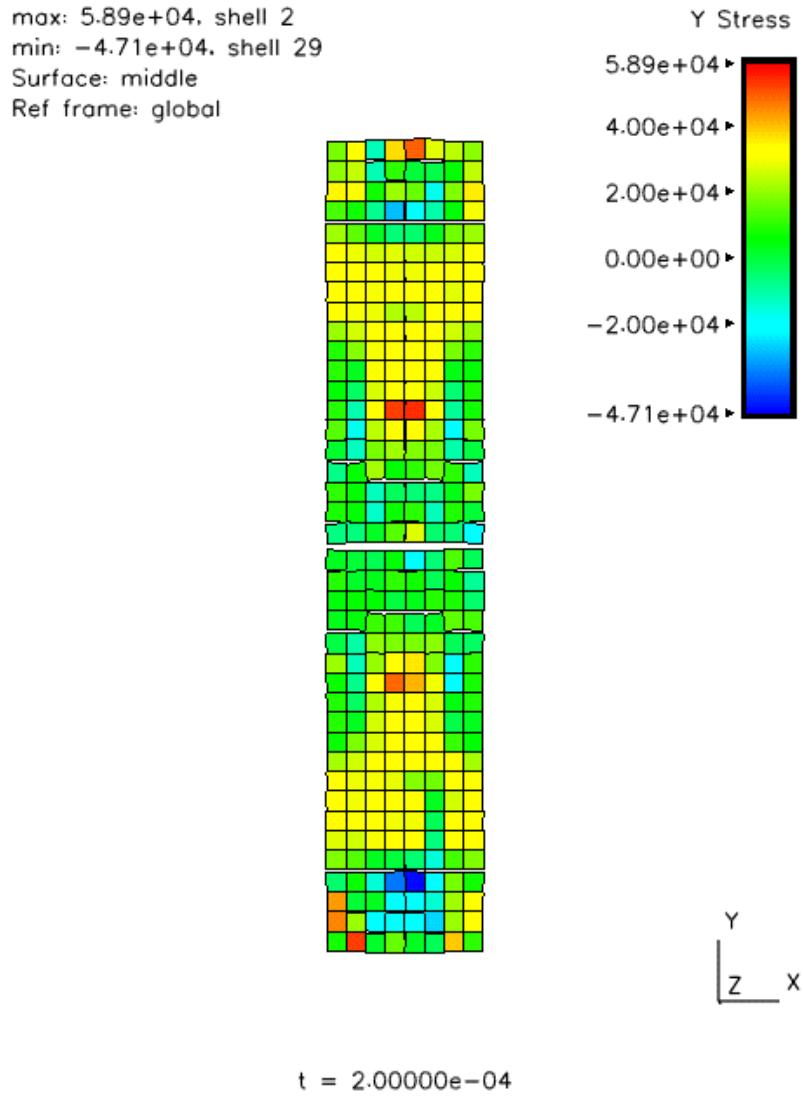

Figure 109. Straight Bar Tension, 320 Elements.

It is noted that the mid-bar failure starting times progressed from 4.91e-05 sec to 4.82e-05 sec to 4.40e-05 sec in this set of three runs which indicates that this failure time is decreasing as the number of elements increase. In all of these runs, the initial starter crack length was held constant at $a_0 = 0.08$ inches while the element sizes ranged from 1.25 inches square, to 0.625 inches square, to 0.3125 inches square.

The next series of simulations conducted using the VFE approach made use of loading Scenario B. In these cases the loading is much more rapid and these cases are characterized by a greater propensity for the end of the bar to spall off than was observed in the Scenario A cases.

Figure 110 shows the Scenario B loading situation for the 20-element simulation. The mid plane fails first at time 3.87e-05 sec followed shortly by the two planes one layer up and down. Finally the top and bottom ends spall off at around 1.46e-04 sec. All of this occurs more quickly than for Scenario A, undoubtedly because of the much steeper loading ramp. The movie for this case is found at Hot Link 110, sbt_b_vfe_20.mov.

Loading Scenario B VFE
Number of Elements: 20 element (2 x 10)
Element Dimension: 1.25” x 1.25”
File Name: /raid5/gerken/frac/rect1/paper_runs/sbt_b_vfe_20

Failures:

vfe number	14 failed, time = 3.8746E-05	vfe number	16 failed, time = 1.1285E-04
vfe number	15 failed, time = 3.8746E-05	vfe number	13 failed, time = 1.1290E-04
vfe number	11 failed, time = 4.0147E-05	vfe number	27 failed, time = 1.4587E-04
vfe number	17 failed, time = 4.0309E-05	vfe number	26 failed, time = 1.4684E-04
vfe number	12 failed, time = 4.0470E-05	vfe number	2 failed, time = 1.47163E-04
vfe number	18 failed, time = 4.0847E-05	vfe number	3 failed, time = 1.47271E-04

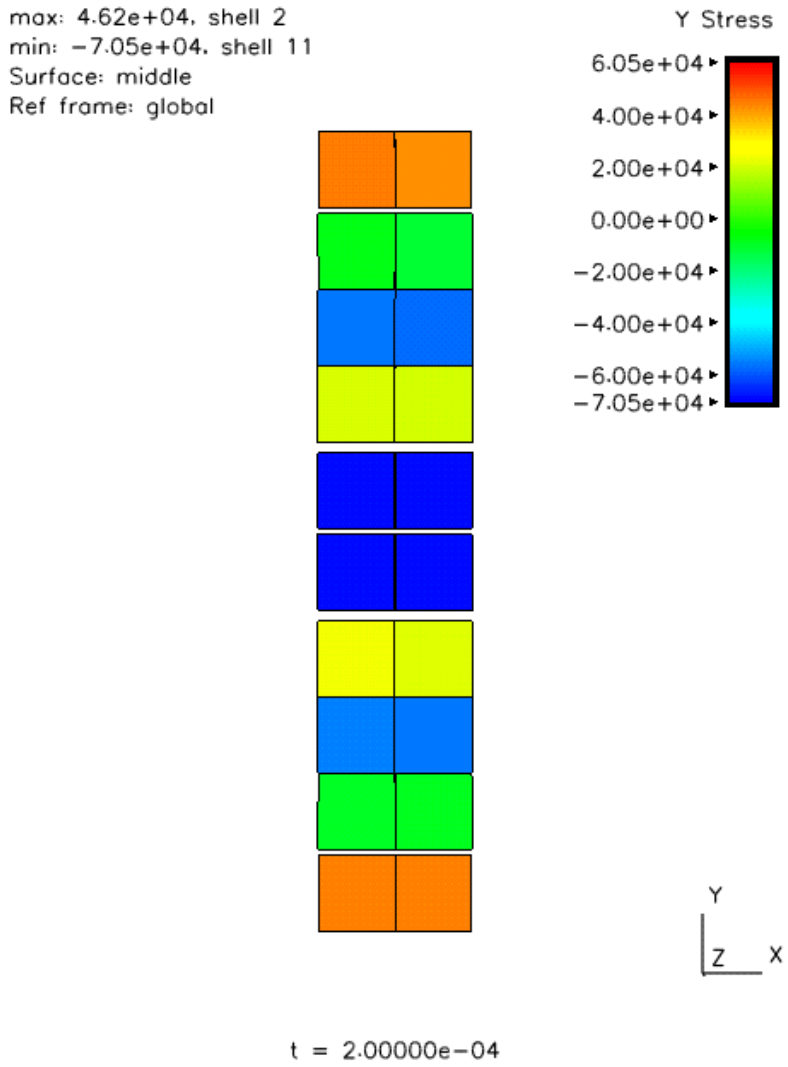

Figure 110. Straight Bar Tension, 20 Elements, Scenario B.

Figure 111 shows the 80-element version of this simulation and the movie is found at Hot Link 111 at sbt_b_vfe_80.mov. In this case the mid-plane failure again occurs first at around time 3.6e-05 sec followed by the two planes up and down one layer. Also, in this case, the end spalls are completed at about 9.5e-05 sec.

Number of Elements:	80 element (4 x 20)
Element Dimension:	0.625" x 0.625"
File Name:	/raid5/gerken/frac/rect1/paper_runs/sbt_b_vfe_80

Failures:

vfe number	68 failed, time = 3.5400E-05	vfe number	76 failed, time = 3.6774E-05
vfe number	70 failed, time = 3.5777E-05	vfe number	47 failed, time = 4.2454E-05
vfe number	67 failed, time = 3.6019E-05	vfe number	90 failed, time = 4.2616E-05
vfe number	60 failed, time = 3.6073E-05	vfe number	131 failed, time = 8.5902E-05
vfe number	69 failed, time = 3.6073E-05	vfe number	6 failed, time = 8.61707E-05
vfe number	75 failed, time = 3.6181E-05	vfe number	5 failed, time = 8.7110E-05
vfe number	62 failed, time = 3.6235E-05	vfe number	132 failed, time = 8.7406E-05
vfe number	77 failed, time = 3.6397E-05	vfe number	4 failed, time = 9.1658E-05
vfe number	63 failed, time = 3.6531E-05	vfe number	133 failed, time = 9.2788E-05
vfe number	61 failed, time = 3.6720E-05	vfe number	130 failed, time = 9.4831E-05
vfe number	74 failed, time = 3.6774E-05	vfe number	7 failed, time = 9.5288E-05

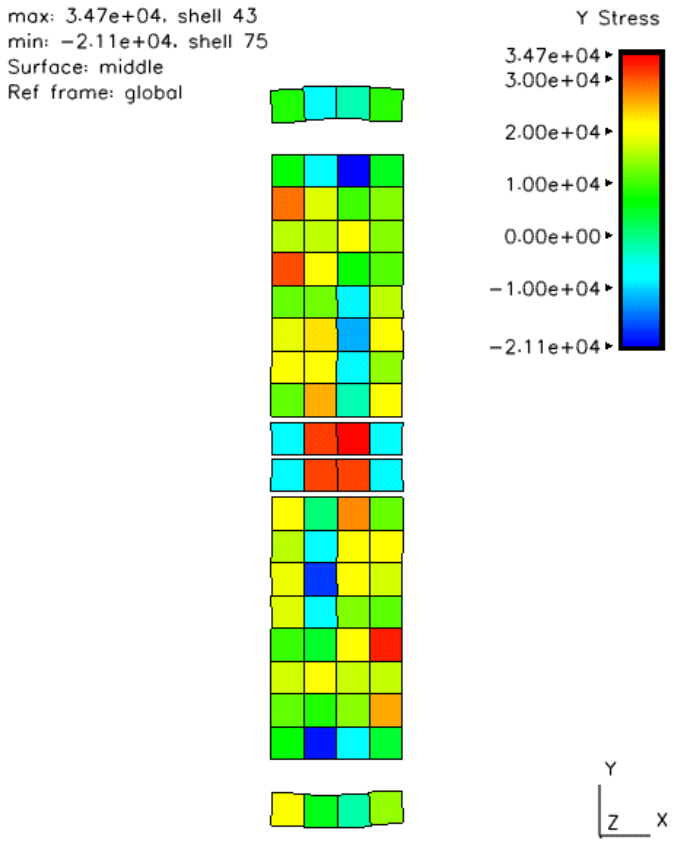

Figure 111. Straight Bar Tension, 80 Elements, Scenario B.

Figure 112 shows the 320-element version of this simulation and Hot Link 112 at sbt_b_vfe_320.mov is the movie of the simulation. In this case the mid-plane starts to fail first, but the planes one layer up and one layer down also start to fail shortly after such that all three planes are failing element-by-element nearly simultaneously. The mid-plane finishes failing at time 3.57e-05 sec while the other two planes finish by 3.59e-05 sec. Then between 7.2 and 7.8e-05 sec, both of the end layers spall off.

Number of Elements:	320 element (8 x 40)
Element Dimension:	0.3125” x 0.3125”
File Name:	/raid5/gerken/frac/rect1/paper_runs/sbt_b_vfe_320

Failures:

vfe number	293 failed, time = 3.5060E-05	vfe number	312 failed, time = 3.5787E-05
vfe number	298 failed, time = 3.5248E-05	vfe number	311 failed, time = 3.5841E-05
vfe number	315 failed, time = 3.5248E-05	vfe number	281 failed, time = 3.5854E-05
vfe number	299 failed, time = 3.5275E-05	vfe number	12 failed, time = 7.2165E-05
vfe number	278 failed, time = 3.5289E-05	vfe number	581 failed, time = 7.2326E-05
vfe number	300 failed, time = 3.5356E-05	vfe number	11 failed, time = 7.2434E-05
vfe number	297 failed, time = 3.5370E-05	vfe number	582 failed, time = 7.2488E-05
vfe number	308 failed, time = 3.5396E-05	vfe number	580 failed, time = 7.2596E-05
vfe number	309 failed, time = 3.5410E-05	vfe number	13 failed, time = 7.2676E-05
vfe number	294 failed, time = 3.5423E-05	vfe number	583 failed, time = 7.2757E-05
vfe number	310 failed, time = 3.5450E-05	vfe number	10 failed, time = 7.2771E-05
vfe number	285 failed, time = 3.5518E-05	vfe number	579 failed, time = 7.3700E-05
vfe number	279 failed, time = 3.5585E-05	vfe number	584 failed, time = 7.3915E-05
vfe number	284 failed, time = 3.5585E-05	vfe number	14 failed, time = 7.4117E-05
vfe number	295 failed, time = 3.5585E-05	vfe number	9 failed, time = 7.4144E-05
vfe number	314 failed, time = 3.5612E-05	vfe number	578 failed, time = 7.7842E-05
vfe number	282 failed, time = 3.5625E-05	vfe number	8 failed, time = 7.7963E-05
vfe number	280 failed, time = 3.5666E-05	vfe number	585 failed, time = 7.8044E-05
vfe number	283 failed, time = 3.5706E-05	vfe number	15 failed, time = 7.8218E-05
vfe number	296 failed, time = 3.5747E-05	vfe number	304 failed, time = 1.8496E-04
vfe number	313 failed, time = 3.5774E-05	vfe number	289 failed, time = 1.8542E-04

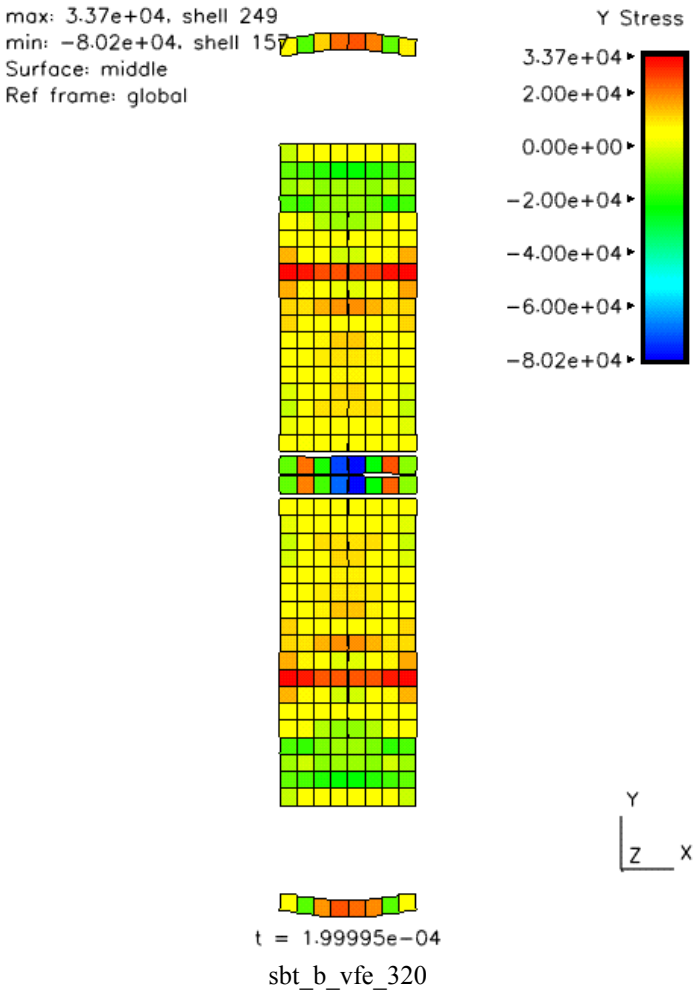

Figure 112. Straight Bar Tension, 320 Elements, Scenario B.

In this set of three simulations, only the top and bottom one-element layers spalled off the ends. In the Scenario A case, which is a less rapid loading scenario, spalling did not occur except in the 320-element case (Figure 109) and in that case a block of elements totaling 1.25 inches in length spalled off.

Again, the mid-bar failure starting times progressed from 3.87e-05 sec, to 3.54e-05 sec, to 3.50e-05 sec as the number of elements increased. In this case, the mid-plane failures start earlier than for Scenario A (time 4.91 to 4.40e-05 sec) probably because the loading ramp for Scenario B is much more rapid. Also in this case, spalling of the ends occurred in each simulation.

Strengths and Weakness of the VFE approach

Strengths: When mini-cracks are present, the VFE approach does model the compliance of such cracks. The original VFE approach models the flow of energy to the crack tip, which energy is the driver of crack growth in each mini-crack. All of the dynamics of the problem are modeled by the FE code, as are the energy flows including strain energy, kinetic energy etc. Even strain rate effects at the crack tip could be included, though that has not been implemented in this work to date. The VFE is capable of modeling straight and curved path cracking processes as long as approximating a curved path by sequential straight segments along the borders of the regular finite elements is acceptable. A simple model for mixed mode behavior is included. The VFE approach eliminates any need to "kill" or remove elements leaving a question about what happened to the mass and energy contained in the "killed" elements.

Weaknesses: Problems occurred with getting the energy calculations to make sense in every test case run. It is not clear exactly why such problems should occur, but it may have to do with the need to select the VFE height "h" and/or the compliance behavior of the VFE elements and the potential associated effects on the wave propagation. With the R-Curve approach, the robustness was improved, but still seemed to be weak overall. It is not certain that the compliance allowed at the element interface was not causing difficulties with the wave propagation and in fact even adding wave propagation effects that are not correct or should not be present. It was found that numerical stability was affected by the relative size of the VFE height "h", so "h" was selected to avoid numerical convergence problems in most of the various test problems considered.

The Tied-node VFE Concept.

The Tied-node approach to the VFE has the potential to eliminate problems associated with the pre-fracture VFE compliance and the need to choose an element height "h" in the original VFE approach. In the Tied-node approach, the node locations in a mesh have multiple nodes as in the VFE approach. However, in this case, a starter crack is assumed to be present at every element interface, but, in this case, the interface crack occurs in a virtual element that has zero thickness. Also, the nodes stay "tied together" as the interface crack grows until the crack has grown to the length of the element interface, at which time the nodes at each end of the interface are released. Before the nodes are

released, the crack is assumed to grow, driven by the strain energy release rate computed from the stress levels present in the neighboring elements.
The stress intensity factors are calculated based upon the stresses at the edge of the neighboring elements and from that the strain energy release rate G can be computed. An R-Curve is used to represent the fracture behavior of the material and the calculated G is entered into the R-Curve, and then is used to predict the change in crack length. The crack length is tracked until the total length reaches the length of the element interface at which time the nodes are released. The Tied-node approach has been developed and tested and shows significant promise. The results of the tests and analyses are discussed in the following sections.

The Tied-Node VFE Formulation

Figures 100 and 101 show the multi-noded mesh that is used for both the VFE and the Tied-Node VFE approach. Figure 113(a) shows Regular Elements A and C with the VFE between and the starter defect is shown to be present in the center of the interface. The node points numbered 1 and 4 are taken to be coincident as are node points 2 and 3. The Tied-Node VFE is taken to have zero height, normal to the interface, and zero mass.

Figure 113(b) shows the crack model used for this VFE. The crack is treated as though it resides in an infinite domain and is subjected to stresses σ_0 and τ_0. For the current work, the remote stresses σ_0 and τ_0 are determined by taking the averages of each from along the edges of the neighboring regular elements A and C. These stresses are then used to compute the Crack Extension Force G from Equations 21, 22 and 23. Then a G R-Curve in the form of Equation 27 is used to determine the amount of crack growth at each time step during the simulation. As the simulation proceeds, the stresses are calculated at each time step for every VFE in the mesh and, through Equations 21, 22, 23 and 27, the R-Curve is used to compute the change in crack size at the end of the time step. The crack size is constrained at each time step so that it cannot shrink in size even if the value of G decreases. The crack size is allowed to increase until the crack length, Figure 113, reaches the element interface length at which time the node pairs 1and 4 along with 2 and 3 are released.

It is important to realize that releasing these two node pairs alone does not fully remove constraint from the mesh and allow a macroscopic crack opening to be modeled. This is true because in general there are four coincident nodes (two node pairs) at these locations as shown in Figure 101. Releasing just one pair of them does not fully release the mesh at that point. Gerken (25) discusses the details of how this process works. Clearly, once the simulation has progressed to the point that both node pairs at a mesh intersection point are released, the crack can then progress on through that point. Gerken (25) also discusses the procedure for releasing nodes in a way that allows cracks to grow vertically or horizontally in meshes such as the one shown in Figure 100. This allows cracks to follow whatever path is dictated by the dynamics of the simulation, albeit along paths approximated by the straight edges of the regular elements.

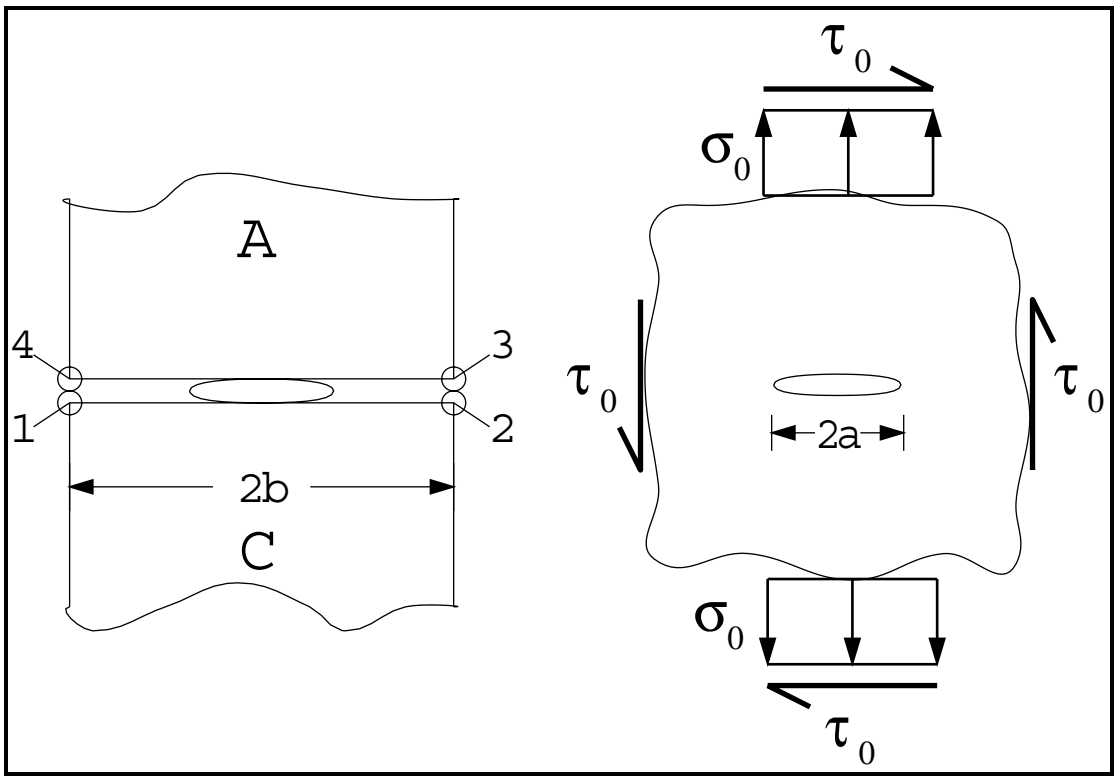

Figure 113. (a) Tied-Node VFE Shown Between Two Neighboring Elements A and C; (b) The Tied-Node VFE with Applied Stresses.

A number of simulations of the sample problem described in Figure 105 were also done in the Tied Node VFE version of the code. The following sections present a discussion of these results.

Figure 114 presents the Tied Node results for the 20 element simulation with loading scenario A. In this case the stress waves propagate to the center of the bar and reinforce causing the bar to fracture at that location. The Tied Node VFE's fail at a time between 4.51 and 4.58 e-05 seconds. The picture shows the bar broken into two pieces at the end of the simulation and the movie at Hot Link 114: sbt_a_tn_20.mov .

Loading Scenario A, Tied Node
Number of Elements: 20 element (2 x 10)
Element Dimension: 1.25” x 1.25”
File Name: /raid5/gerken/frac/rect1/paper_runs/sbt_a_tn_20
Failure:

```
vfe number          14 failed, time =  4.5119219012639384E-05
vfe number          15 failed, time =  4.5873646373067462E-05
```

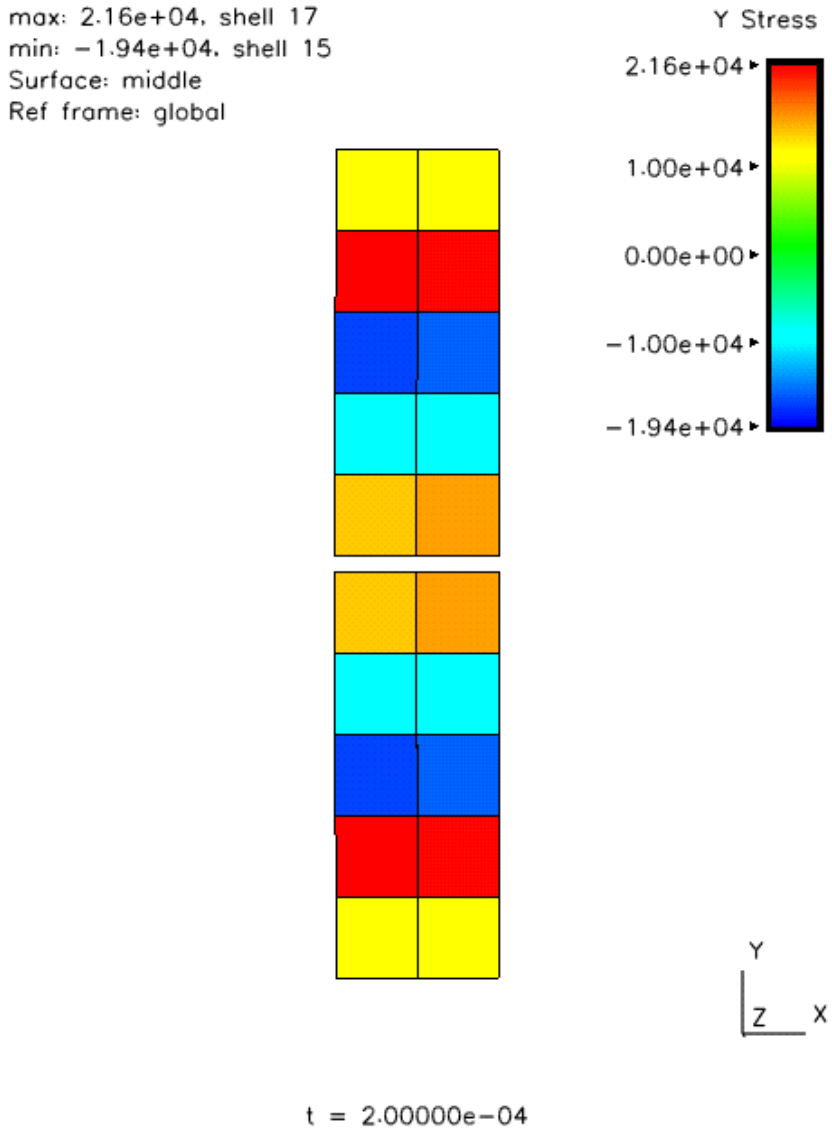

sbt_a_tn_20

Figure 114. Straight Bar Tension, 20 Elements, Scenario A.

Figure 115 presents the results for the Tied Node simulation with 80 elements and loading scenario A. In this case, the failures begin one layer down from the center of the bar at time 4.66 e-05 seconds rather than exactly at the center of the bar. One layer up begins fracturing at about the same time and both of these layers have finished fracturing by time 4.94 e-05 seconds. The center layer has two elements fail at around time 6.11 e-05 seconds, but the center plane does not completely fail. Also by the time the two layers that fail completely have finished failing, two elements at levels two layers up and two layers down from the center have also failed. In addition, it is interesting that in this case a number of vertically oriented VFE's fail around the center area of the bar in a symmetrically arranged pattern. These failures begin at about time 6.09 e-05 seconds. The movie of this simulation can be viewed at Hot Link 115: sbt_a_tn_80.mov .

Loading Scenario A, Tied Node.
Number of Elements: 80 element (4 x 20)
Element Dimension: 0.625” x 0.625”
File Name: /raid5/gerken/frac/rect1/paper_runs/sbt_a_tn_80
Failure:

```
vfe number 61 failed, time =  4.665E-05
vfe number 62 failed, time =  4.665E-05
vfe number 75 failed, time =  4.665E-05
vfe number 76 failed, time =  4.665E-05
vfe number 53 failed, time =  4.902E-05
vfe number 56 failed, time =  4.902E-05
vfe number 81 failed, time =  4.902E-05
vfe number 84 failed, time =  4.902E-05
vfe number 60 failed, time =  4.923E-05
vfe number 63 failed, time =  4.923E-05
vfe number 74 failed, time =  4.923E-05
vfe number 77 failed, time =  4.923E-05
vfe number 65 failed, time =  6.093E-05
vfe number 72 failed, time =  6.096E-05
vfe number 68 failed, time =  6.115E-05
vfe number 69 failed, time =  6.115E-05
vfe number 78 failed, time =  9.234E-05
vfe number 80 failed, time =  9.234E-05
vfe number 57 failed, time =  9.237E-05
vfe number 59 failed, time =  9.237E-05
```

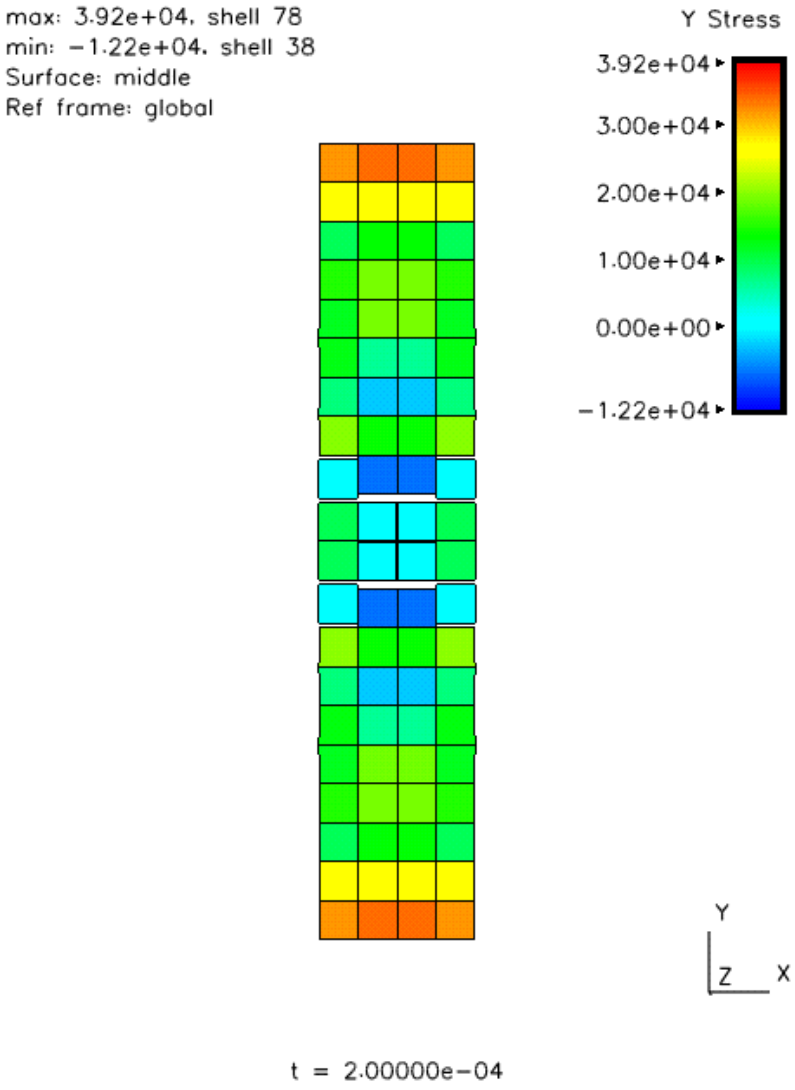

Figure 115. Straight Bar Tension, 80 Elements, Scenario A.

Figure 116 shows the results for a simulation with 320 elements with load scenario A. In this case the bar breaks near the center of the bar but with two fractures, one that is two layers up from the center and one that is two layers down from the center. The two fractured layers have completed fracturing by about time 4.99 e-05 seconds, but while that was occurring, four element symmetrically located four layers up and down on the edges had also failed. After the two horizontal layers completed separation, two elements in the center of the middle layer then separated and two vertically oriented VFE's failed on the vertical centerline of the bar two layers up and two down. The movie of this simulation can be viewed at Hot Link 116: sbt_a_tn_320.mov .

Loading Scenario A, Tied Node.
Number of Elements: 320 element (8 x 40)
Element Dimension: 0.3125” x 0.3125”
File Name: /raid5/gerken/frac/rect1/paper_runs/sbt_a_tn_320
Failure:

```
vfe number 266 failed, time =  4.543E-05
vfe number 267 failed, time =  4.543E-05
vfe number 326 failed, time =  4.543E-05
vfe number 327 failed, time =  4.543E-05
vfe number 265 failed, time =  4.593E-05
vfe number 268 failed, time =  4.593E-05
vfe number 325 failed, time =  4.593E-05
vfe number 328 failed, time =  4.593E-05
vfe number 264 failed, time =  4.757E-05
vfe number 269 failed, time =  4.757E-05
vfe number 324 failed, time =  4.757E-05
vfe number 329 failed, time =  4.757E-05
vfe number 233 failed, time =  4.808E-05
vfe number 240 failed, time =  4.808E-05
vfe number 353 failed, time =  4.810E-05
vfe number 360 failed, time =  4.810E-05
vfe number 323 failed, time =  4.991E-05
vfe number 330 failed, time =  4.991E-05
vfe number 263 failed, time =  4.993E-05
vfe number 270 failed, time =  4.993E-05
vfe number 296 failed, time =  5.861E-05
vfe number 297 failed, time =  5.861E-05
vfe number 319 failed, time =  5.878E-05
vfe number 274 failed, time =  5.882E-05
```

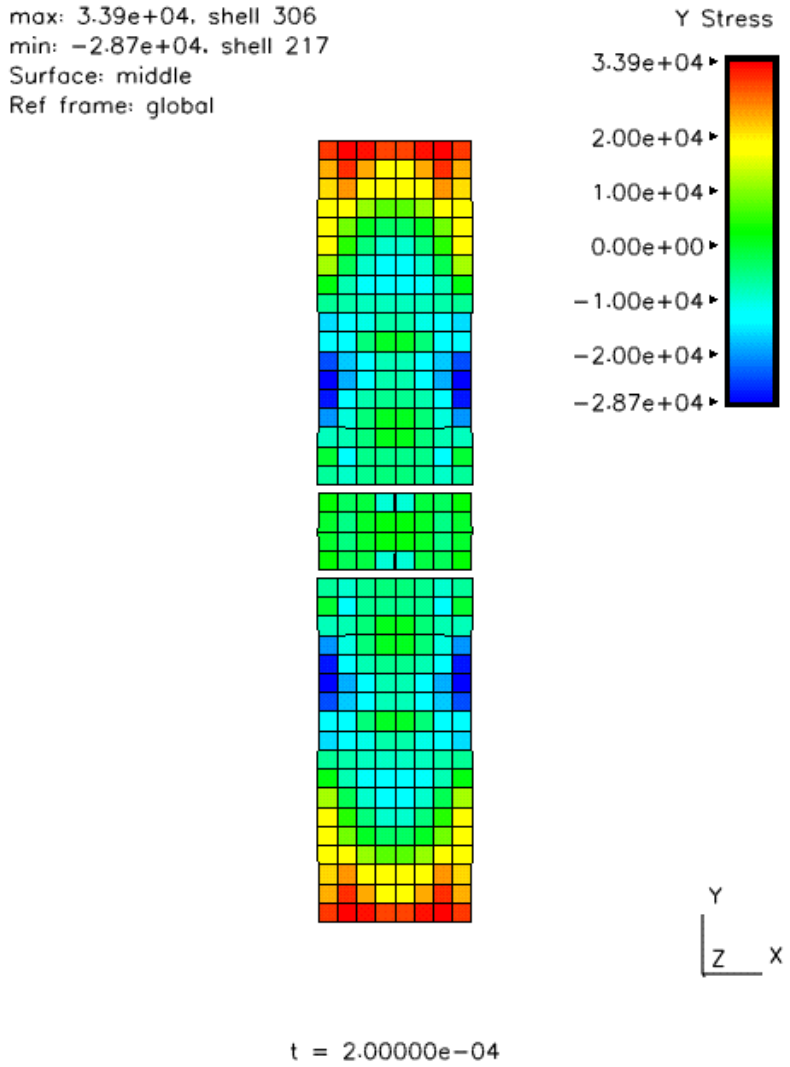

Figure 116. Straight Bar Tension, 320 Elements, Scenario A.

Figure 117 shows the Straight Bar Tension test problem with twenty elements and loading scenario B, the more aggressive loading ramp. In this case the middle layer of VFE's break and separate the bar into two pieces at time 3.59 e-05 seconds. The two ends spall off at time 1.63 e-04 seconds. The movie of this simulation can be viewed at Hot Link 117: sbt_b_tn_20.mov .

Loading Scenario B, Tied Node.
Number of Elements: 20 element (2 x 10)
Element Dimension: 1.25" x 1.25"
File Name: /raid5/gerken/frac/rect1/paper_runs/sbt_b_tn_20
Failure:

```
vfe number 14 failed, time =  3.594E-05
vfe number 15 failed, time =  3.594E-05
vfe number 2 failed, time =  1.630E-04
vfe number 3 failed, time =  1.630E-04
vfe number 26 failed, time =  1.631E-04
vfe number 27 failed, time =  1.631E-04
```

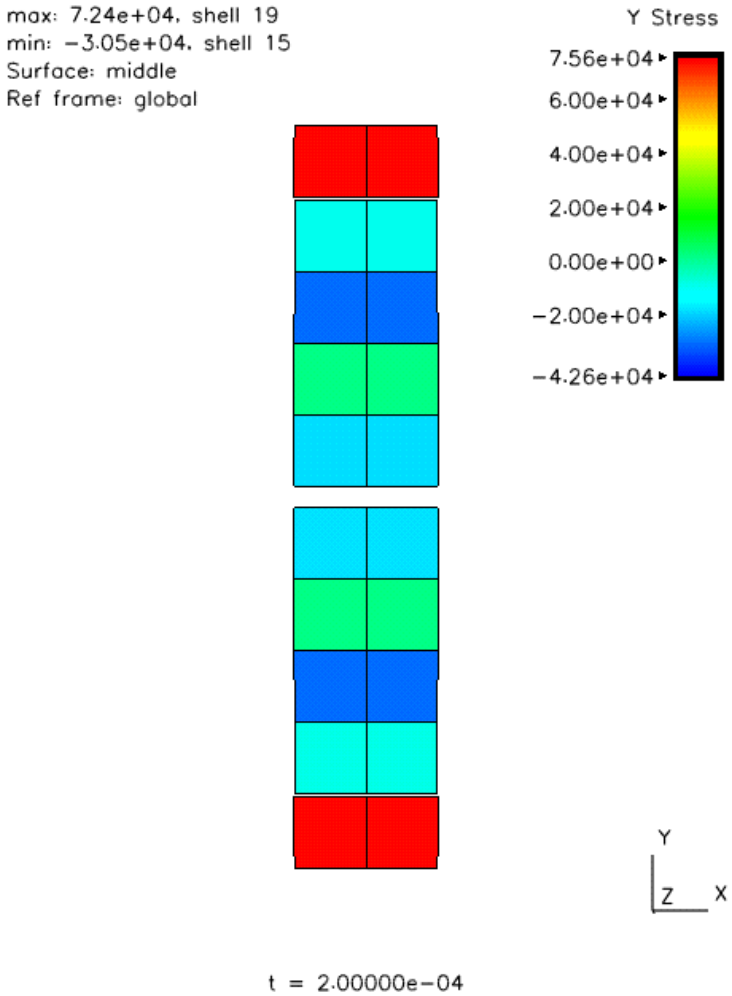

Figure 117. Straight Bar Tension, 20 Elements, Scenario B.

Figure 118 shows the straight tension bar for the case with eighty elements and loading scenario B. By time 3.42 e-05 seconds, the middle plane has fractured along with a few edge VFE's and four vertically oriented VFE's oriented symmetrically above and below the middle of the bar. Between time 1.55 e-04 seconds and time 1.62 e-04 seconds, the top and bottom ends of the bar spall off. The movie of this simulation can be viewed at Hot Link 118: sbt_b_tn_80.mov .

Loading Scenario B, Tied Node.
Number of Elements: 80 element (4 x 20)
Element Dimension: 0.625" x 0.625"
File Name: /raid5/gerken/frac/rect1/paper_runs/sbt_b_tn_80
Failure:

vfe number 67 failed, time = 3.386E-05	vfe number 71 failed, time = 7.893E-05
vfe number 70 failed, time = 3.386E-05	vfe number 73 failed, time = 7.893E-05
vfe number 68 failed, time = 3.416E-05	vfe number 11 failed, time = 1.550E-04
vfe number 69 failed, time = 3.416E-05	vfe number 14 failed, time = 1.550E-04
vfe number 60 failed, time = 3.427E-05	vfe number 123 failed, time = 1.550E-04
vfe number 63 failed, time = 3.427E-05	vfe number 126 failed, time = 1.550E-04
vfe number 74 failed, time = 3.427E-05	vfe number 12 failed, time = 1.629E-04
vfe number 77 failed, time = 3.427E-05	vfe number 13 failed, time = 1.629E-04
vfe number 64 failed, time = 7.893E-05	vfe number 124 failed, time = 1.629E-04
vfe number 66 failed, time = 7.893E-05	vfe number 125 failed, time = 1.629E-04

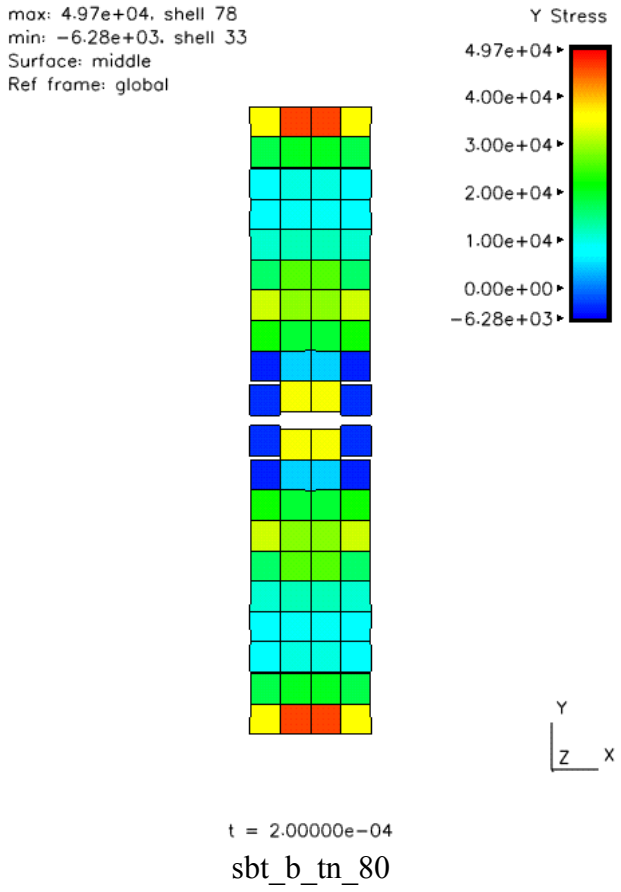

Figure 118. Straight Bar Tension, 80 Elements, Tied Node, Loading Scenario B.

Figure 119 shows the straight bar with loading scenario B and 320 elements. Here the midplane fractures at time 3.25 e-05 seconds and there are some failures above an below the mid-plane at the same time. The two ends spall off starting at 8.85e-5 seconds and ending by 9.90e-5 seconds. The movie of this simulation can be viewed at Hot Link 119: sbt_b_tn_320.mov .

Loading Scenario B, Tied Node.
Number of Elements: 320 element (8 x 40)
Element Dimension: 0.3125" x 0.3125"
File Name: /raid5/gerken/frac/rect1/paper_runs/sbt_b_tn_320
Failure:

The vfe failure file for this run is not available.

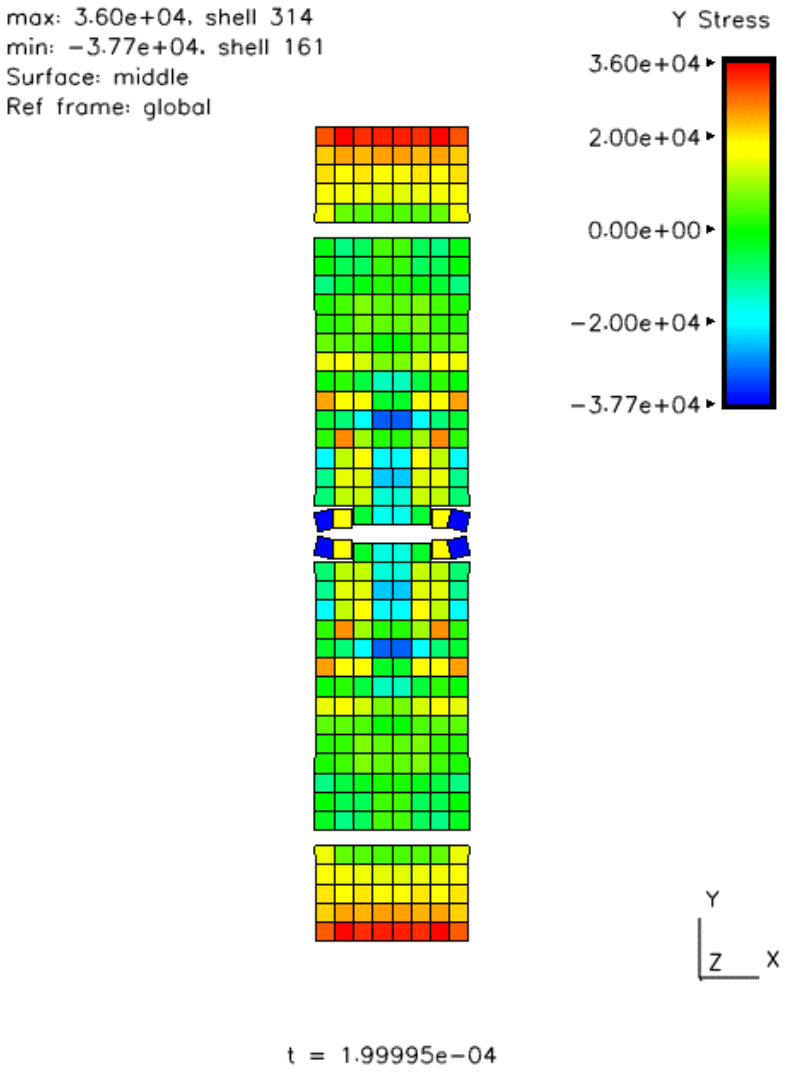

Figure 119. Straight Bar Tension, 320 Elements, Scenario B.

Figures 114 through 119 and their associated movies constitute the test cases for the Tied Node VFE approach in DYNA3D conducted so far. Before these are discussed further, a set of simulations using the ICE (Interface Crack Element) approach developed for ABAQUS implementation by Gerken (25) will be presented. These are presented for purposes of comparison with the results on the Straight Bar Tension problem obtained from the VFE and the Tied Node VFE formulations that were implemented in DYNA3D. Movies for the ICE simulations are, however, not available. The ICE simulations were all conducted using the same R-Curve, specimen geometry and loading conditions discussed so far and presented in Figure 105.

Figures 120 through 122 present the ICE simulations for the straight bar tension specimen subjected to loading scenario A. The file containing the times at which various interface cracks failed is not available for presentation in these figures, but comments are provided in each figure describing the times at which important events were observed to occur.

Number of Elements:	20 element (2 x 10)
Element Dimension:	1.25” x 1.25”
File Name:	/raid5/gerken/abqus/paper_run/sbt_a_ice_20
Failure:	

Notes: Mid-plane failure occurs at 4.65e-05 seconds

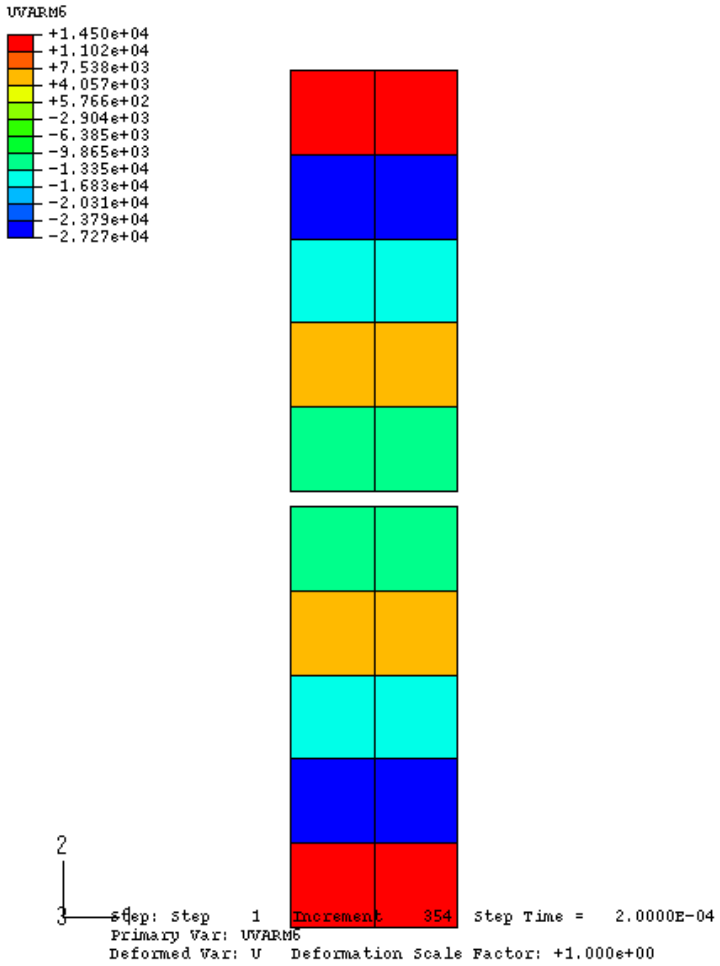

Figure 120. Straight Bar Tension, 20 Elements, ICE, Loading Scenario B.

Number of Elements:	80 element (4 x 20) Loading Scenario A
Element Dimension:	0.625” x 0.625”
File Name:	/raid5/gerken/abqus/paper_run/sbt_a_ice_80
Failure:	

Mid-plane failure starts 4.65e-05 seconds. Failures in layers that are 2 up and 2 down start at 4.95e-5. Center area fracture ends by 5.05e-5. Edge elements break at center of remaining fragment at 1.02e-4

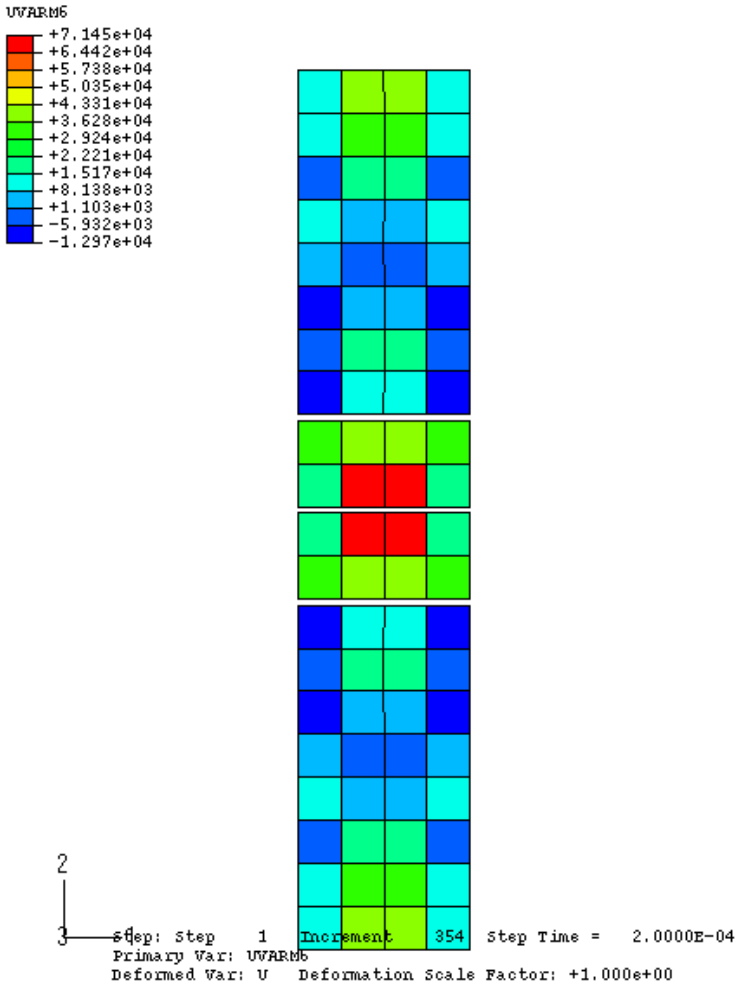

Figure 121. Straight Bar Tension, 80 Elements, ICE, Loading Scenario B.

Number of Elements:	320 element (8 x 40) Loading Scenario A
Element Dimension:	0.3125” x 0.3125”
File Name:	/raid5/gerken/abqus/paper_run/sbt_a_ice_320
Failure:	

Failure started at the center two elements of the mid-plane at 4.65e-5 seconds. That was immediately followed by shattering above and below the mid-plane. Separation into two pieces occurred at 7.6e-5. Spalling of the end 4 rows of elements starts at about 1.02e-4 seconds. Spalling was not expected to occur in this simulation.

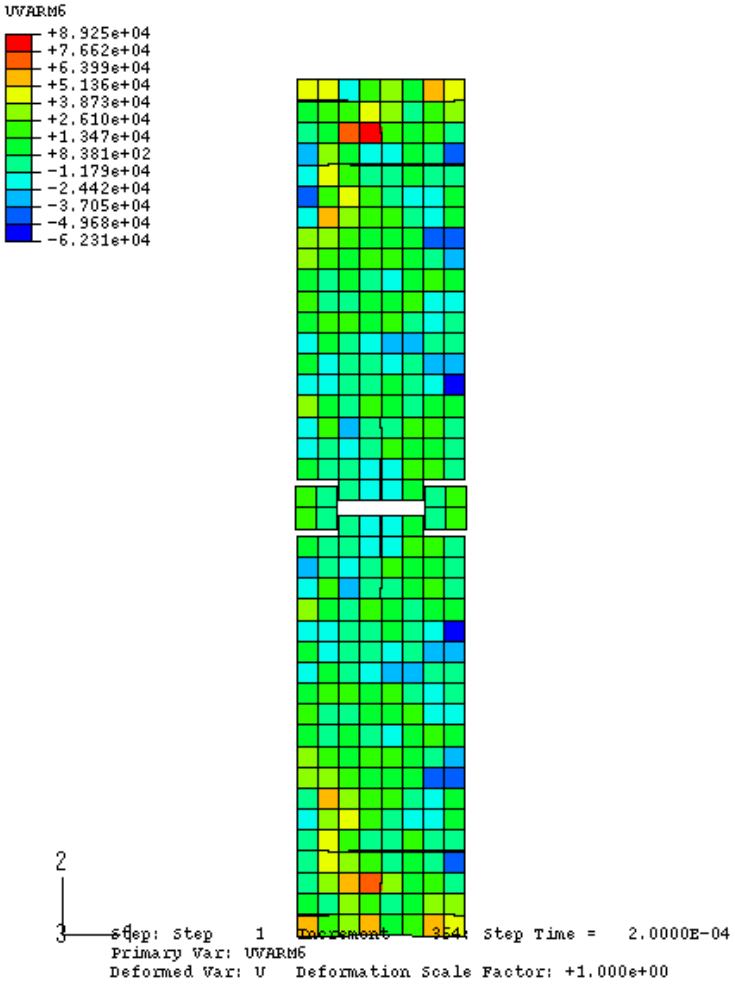

Figure 122. Straight Bar Tension, 320 Elements, ICE, Loading Scenario B.

Figures 123 through 125 give the results of ICE simulations for the straight bar tension specimen subjected to loading scenario B. In this case it expected that the ends of the bars should spall off after the mid-plane fails or after multiple failures in and around the mid-plane occur. In these figures, the ends spalled off in every case, but it is not easy to see in every case.

Number of Elements: 20 element (2 x 10)
Element Dimension: 1.25" x 1.25"
File Name: /raid5/gerken/abqus/paper_run/sbt_b_ice_20
Failure: The mid-plane and 1 row up and 1 row down all fail at 3.65e-5 seconds. Both ends spall off at 1.785e-4 seconds.

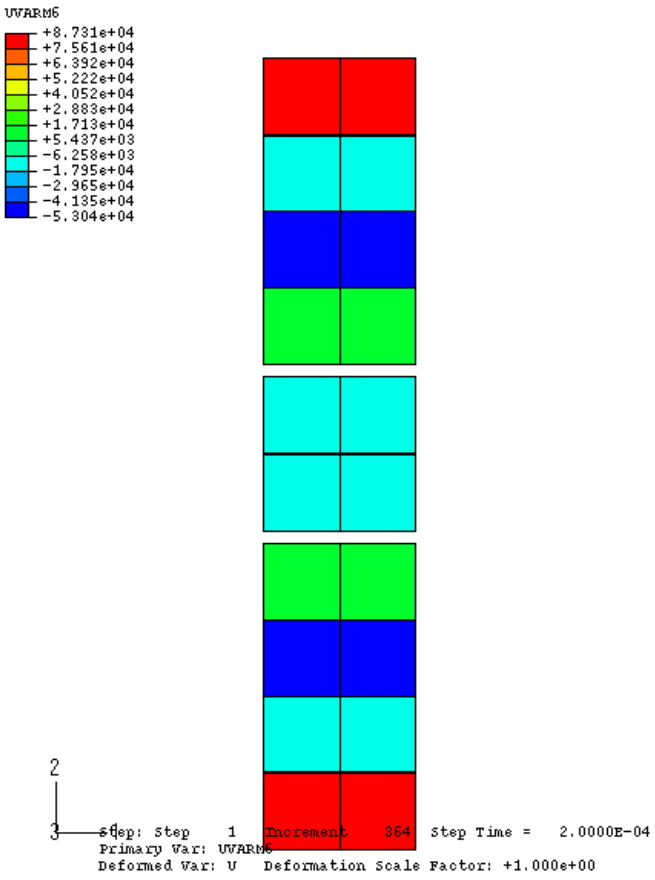

Figure 123. Straight Bar Tension, 20 Elements, ICE, Loading Scenario B.

Number of Elements:	80 element (4 x 20) Loading Scenario B
Element Dimension:	0.625” x 0.625”
File Name:	/raid5/gerken/abqus/paper_run/sbt_b_ice_80

Failure: Failure starts on the outside two elements, one row up and one row down from the mid-plane at 3.45e-5 seconds. The mid-plane starts to fail at 3.5e-5 seconds in the center two elements. Failure starts on the interior 2 elements, 2 rows up and 2 rows down from the mid-plane at 3.65e-5 seconds. Failure starts on the exterior two elements 3 rows up and 3 rows down at 3.8e-5 seconds. Complete separation of the 2 rows up and 2 rows down occurs at 4.5e-5 seconds. Complete separation of the mid-plane occurs at 8.05e-5 seconds. Spall of the end two rows of elements starts in the outer two elements at 1.024e-4 seconds and is complete at 1.08e-4 seconds. Note: The simulation crashed at 1.28e-4 seconds.

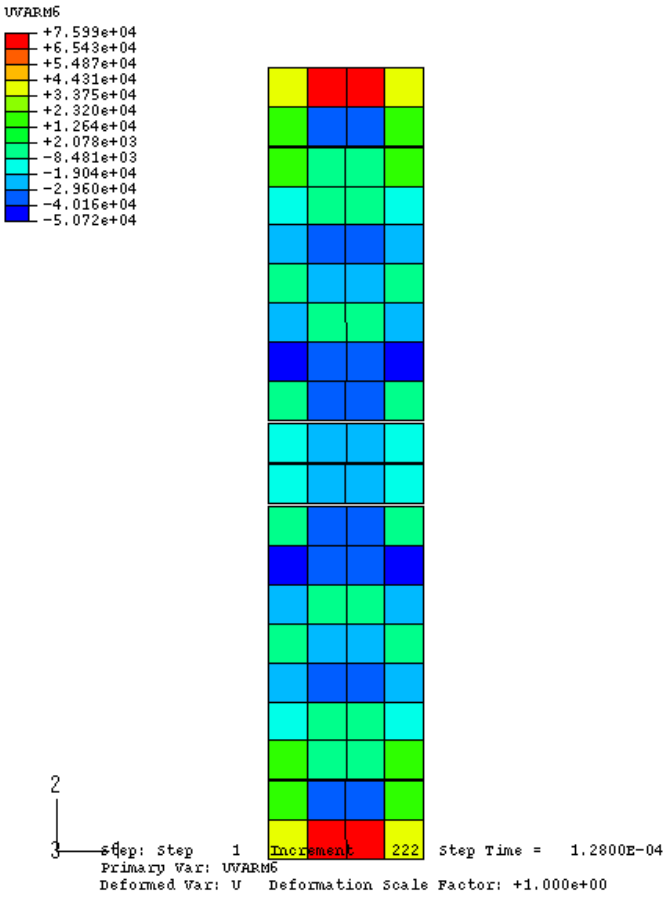

Figure 124. Straight Bar Tension, 80 Elements, ICE, Loading Scenario B.

Number of Elements:	320 element (8 x 40) Loading Scenario B
Element Dimension:	0.3125” x 0.3125”
File Name:	/raid5/gerken/abqus/paper_run/sbt_b_ice_320

Failure: Mid-plane failure starts at 3.15e-5 seconds and finishes at 3.2e-5 seconds. Fracture of the center 2 interfaces 4 rows from the mid-plane occur at 3.65e-5 seconds. Failure of the outer elements 6 rows from the mid-plane start to occur at 3.85e-5 seconds. The center two elements on the two edges fracture at 5.6e-5 seconds (start of spall of the end pieces). Complete fracture of the interfaces 6 rows from the mid-plane occurs by 9.5e-5. End spall is complete by 1.07e-4 seconds.
Also note that this picture is not at 2e-4 seconds. This is because the solution crashed at the time just after this print-out.

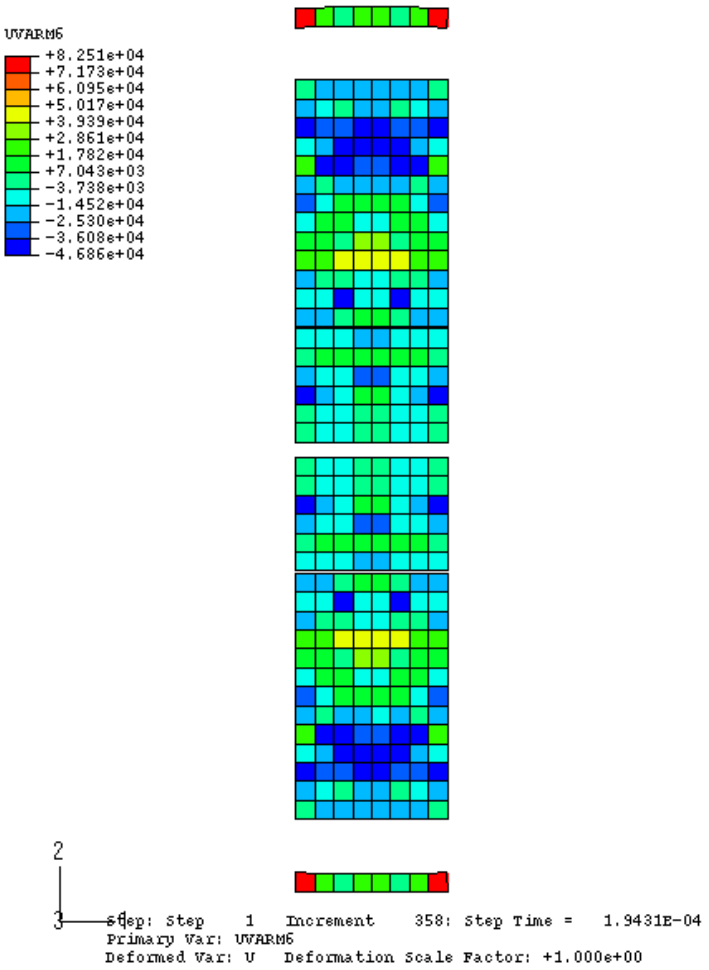

Figure 125. Straight Bar Tension, 320 Elements, ICE, Loading Scenario B.

Discussion of Straight Bar Tension Results.

Results have been presented from three different numerical approaches all applied to the same problem. In all cases, the initial starting crack size was 0.08 inches. The VFE and Tied-Node VFE approaches were implemented in DYNA3D while the ICE approach was implemented in ABAQUS standard.

Table 101 presents a summary of the results for both loading scenarios. The time of first failure of any VFE is given as is the time of first failure of a mid-plane VFE. The column entitled SPALL gives comments about spalling of the ends and, where relevant, the time at which the spall failure initiates is given.

Table 101. Summary of Straight Bar Tension Results

Loading Scenario	Virtual Element Type	Number of Regular Elements	Time of First Failure Sec.	Mid-plane Failure Starts, Sec.	Ends Spall at Time in sec.
A	VFE	20	4.91e-05	4.91e-05	No Spall
A	TN-VFE	20	4.51e-05	4.51e-05	No Spall
A	ICE	20	4.65e-05	4.65e-05	No Spall
A	VFE	80	4.83e-05	4.98e-05	Spall 10e-05
A	TN-VFE	80	4.66e-05	6.11e-05	No Spall
A	ICE	80	4.65e-05	4.65e-05	No Spall
A	VFE	320	4.40e-05	4.40e-05	Spall 1.55e-04
A	TN-VFE	320	4.54e-05	5.86e-05	No Spall
A	ICE	320	4.65e-05	4.65e-05	Spall 1.02e-04
B	VFE	20	3.87e-05	3.87e-05	Spall 1.46e-04
B	TN-VFE	20	3.59e-05	3.59e-05	Spall 1.63e-04
B	ICE	20	3.65e-05	3.65e-05	Spall 1.78e-04
B	VFE	80	3.54e-05	3.54e-05	Spall 8.59e-05
B	TN-VFE	80	3.39e-05	3.39e-05	Spall 1.55e-05
B	ICE	80	3.45e-05	3.50e-05	Spall 1.02e-04
B	VFE	320	3.51e-05	3.51e-05	Spall 7.21e-05
B	TN-VFE	320	3.25e-05	3.25e-05	Spall 8.85e-05
B	ICE	320	3.15e-05	3.15e-05	Spall 5.60e-05

The dynamically loaded straight bar considered here is a complicated problem and not one that has simple analytical solutions with which to easily compare, so such comparisons are not attempted at this writing. Some general statements can be made that indicate the codes are behaving in ways that predict somewhat consistent behavior for these problems. This can be seen by examination of the times to first failure as presented in Figure 126. The times of first failure for Scenario A range between 44.0 and 49.1 microseconds while the times of first failure for Scenario B range between 31.5 and 38.7 microseconds. The predicted time of first failure are shorter for Scenario B because the loading reaches the maximum load sooner and because the value of the maximum load is

larger for Scenario B. Behavior consistent with convergence due to element size decrease is not expected to occur in these results. That is true because these problems all have macroscopic cracks present that are of constant size and as the elements shrink, the cracks become a larger portion of the element size. Still, the time of first failure predicted by the three techniques are consistent with each other as the number of elements increase and their sizes decrease.

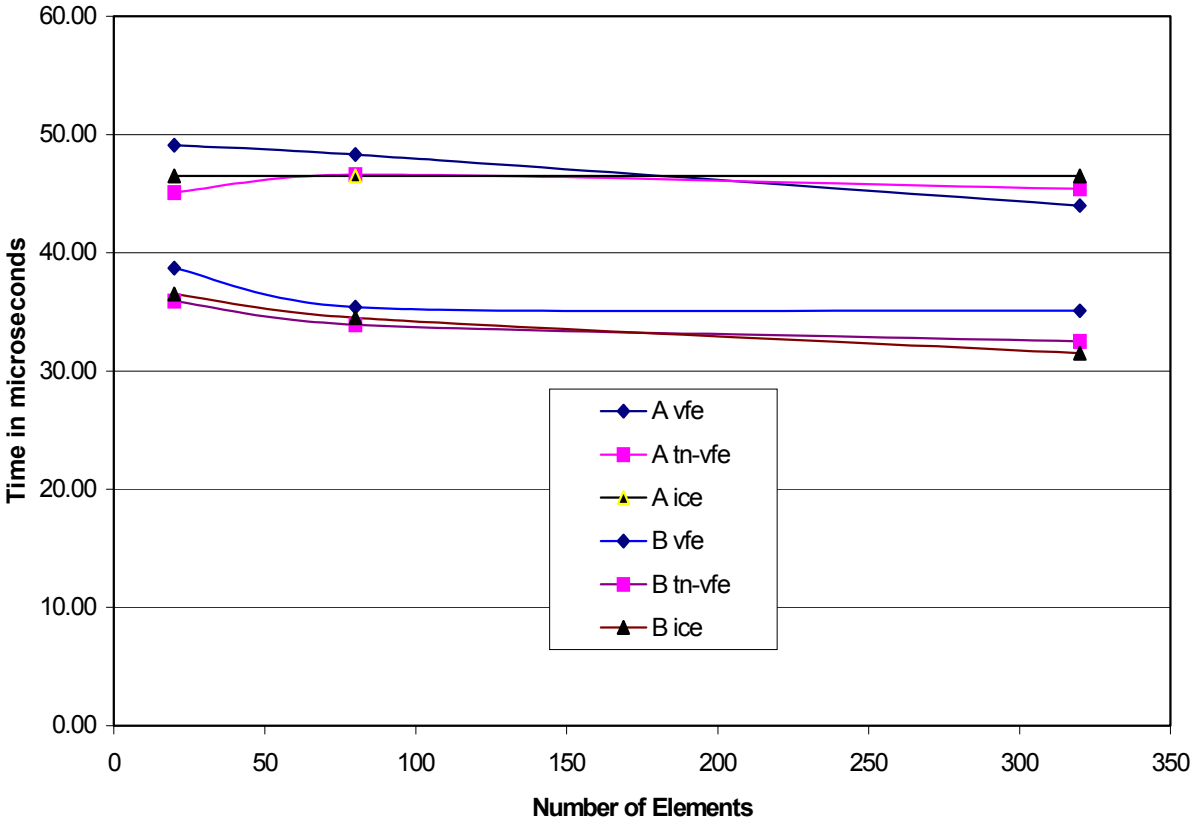

Figure 126. Time of First Failure in Straight Bar Tension Simulations. A and B denote Scenario A and B respectively.

In Table 101 it is noted that every one of the Scenario B cases demonstrates a spall failure at the ends while most of those in Scenario A do not. The two scenarios were pre-selected by noticing, during practice analysis runs, that there appeared to be a dividing line between spalling or not spalling based on the steepness of the loading ramp and the magnitude of the maximum load applied. It turned out however, that in Scenario A with 80 elements and with 320 elements, that spalling is predicted in some of the runs. It is important to remember that the formulations of the three analysis approaches are different from each other, so some differences in the predictions are not surprising.

These differences show up not only in the spalling behavior at the ends, but also in the nature of the first failure. In some cases, the first failure is at the mid-plane and it progresses smoothly across the mid-plane to separate the bar into two pieces. In other cases, the first failure occurs away from the mid-plane, but still near the mid-plane of the bar and progresses into a kind of shattering of the middle part of the bar on more than one plane. While these behaviors are not the same, they are indeed similar. However, in the absence of experimental results to use for comparison, not much further can be said about these results.

It is encouraging that the predicted times of first failure are somewhat similar in Scenario A for the three different analysis approaches as is the case for Scenario B. Further, it is also encouraging that all three of the analysis approaches predict the same trend in time of first failure when changing from Scenario A to Scenario B.

The Stout-Liu Cantilever Impact Experiment

To study the behavior of High Explosives, Stout and Liu (26) developed an impact experiment as shown in Figure 127. The impact of this experiment was simulated using both the tied node VFE and the ICE discrete fracture models. The setup, shown in the figure, consisted of a 6" x 3" piece of A2 tool steel clamped at one end. A notch 1" long is located in the center of the lower edge of the specimen as shown. A load is applied to the cantilever via a compressive stress wave traveling through a long rod in contact with the edge of the specimen. The simulation uses the material properties for steel with E = 30E+06 psi and $\nu = 0.29$. The R-curve was estimated from Fracture Toughness data given by Crane and Bigg (27) for the A2 tool Steel used in the experiment and is given by

$$G = 16(\Delta a)^{0.75} + 10 \qquad (29)$$

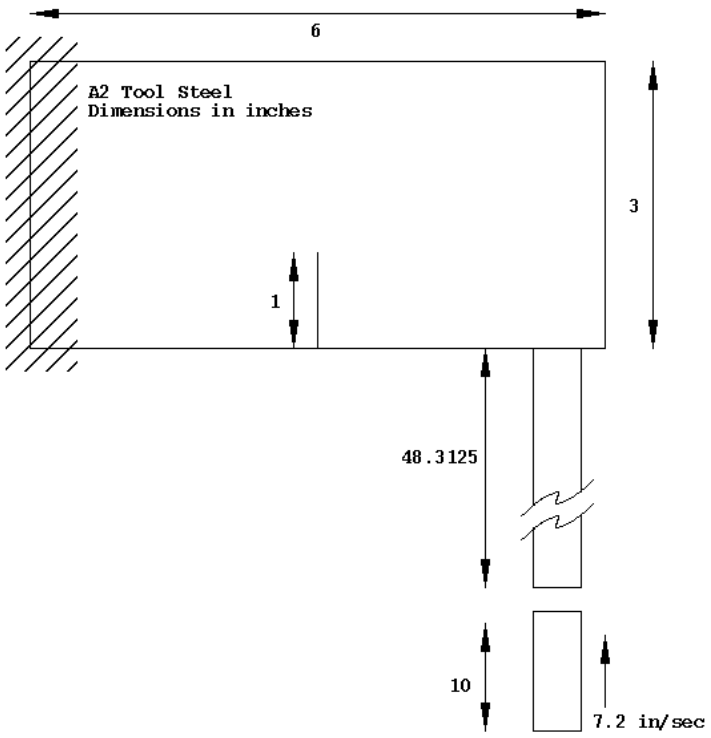

Figure 126. Setup of A2 tool steel cantilever impact experiment.

The ten-inch impact slug was initially travelling with a speed of 7.2 inches per second as shown in Figure 126. It hit the end of the long bar and caused a stress wave to propagate along the bar and into the cantilever specimen. The resulting waves interacted in a complex way with the specimen and the crack tip and caused the specimen to fracture into two parts after the crack propagated completely through the sample. Figure 128 shows a tracing made from the broken parts after completion of the experiment. The wavy line in the tracing represents the path along which the crack propagated during the experiment. The crack meandered slightly left for about 1.5 inches then turned sharply to the left and propagated toward the clamp. As the crack neared the clamp it turned sharply again, exiting the specimen at the top edge near the clamp. Data on crack speed are not available from the experiment.

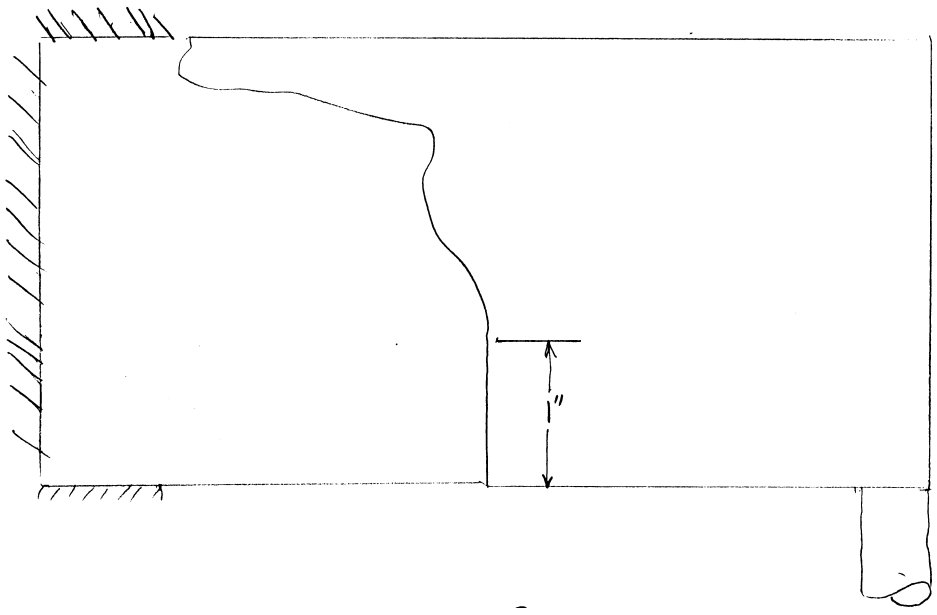

Figure 128. Tracing of crack path after failure. Made by Smith, Gerken, Liu, Stout, June 11, 1998.

Figure 129 shows the final state in a simulation of the Stout Liu Cantilever experiment using the Tied Node VFE approach. Equation 29 was used for the G R-Curve. The crack started to grow at time 7.97e-05 seconds. A movie of this simulation can be viewed at Hot Link 129: cantilever mov tn.091799.qt . Examination of the movie indicates that the crack moves straight ahead for a time then turns left in a way similar to what occurred in the experiment.

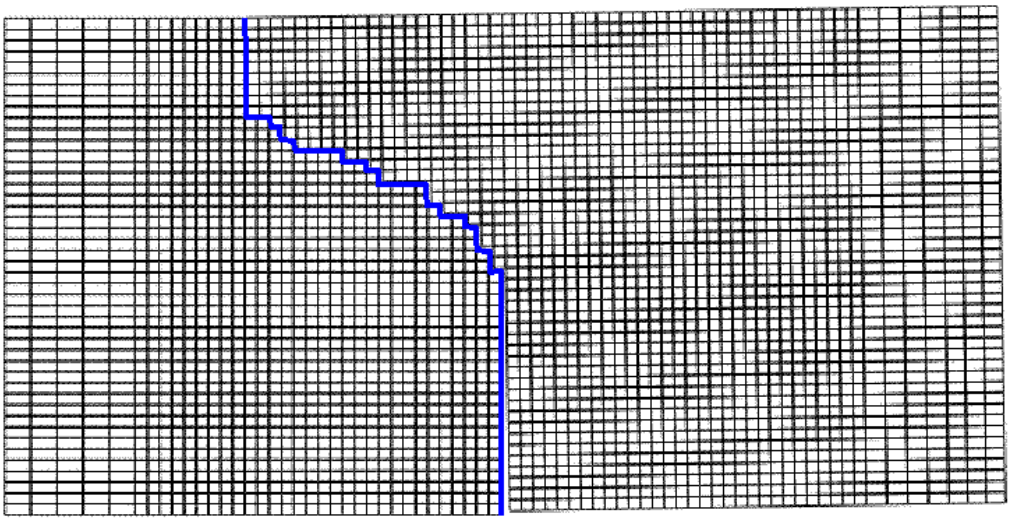

Figure 129. Tied Node VFE Simulation of the Stout Liu Cantilever Experiment.

Figure 130 shows the final state in a simulation of the same problem using the ICE approach, shown in pink. The crack path from the experiment is shown in red and the crack path from the Tied Node simulation is repeated here in blue. Again, the crack path from the simulation is quite similar to the crack path determined from the experiment. The movie of this simulation may be viewed at Hot Link 130: cantilever mov ice.mov .

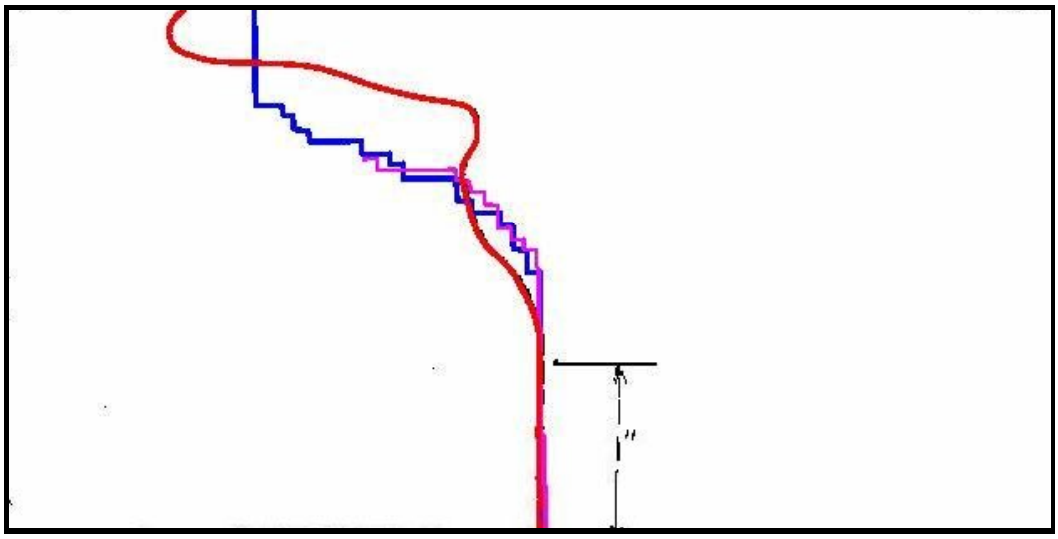

Figure 130. ICE Simulation of the Stout Liu Cantilever Experiment Superimposed on the Experimental Crack Path and Tied Node Results. Blue = Tied Node Simulation, Red = Experimental Crack Path, Pink = ICE Simulation.

These simulations give crack path results that are similar to each other and similar to the experimental crack path. This comparison lends credibility to both the ICE and Tied Node VFE approaches through comparison with this validation experiment.

Straight Bar Spall Simulation

Figure 131 shows steel bar, with dimensions L = 12.5 in., W = 2.5 in., and t = 0.1 in., that is impacted by a steel projectile with length, l = 0.25 in., and velocity, V = 1092.9 in/sec.

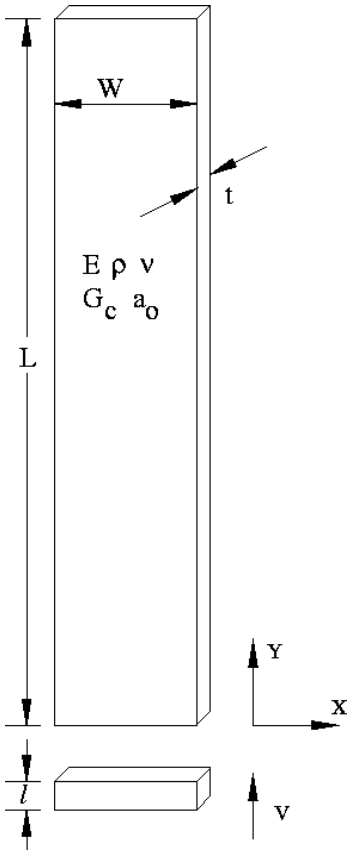

Figure 131. A thin bar impacted by a short thin projectile.

The simulation assumes perfect transmission of the compressive wave from the projectile into the bar until a tensile release wave reaches the contact interface at which point perfect unloading occurs over a finite time. The stress at the interface can be calculated from the equation $\sigma = \rho c v$, where σ is the stress, ρ is the density of the material, c is the longitudinal wave speed in the material, and v is the velocity of the impactor. The time of transmission of the compressive wave from the impactor to the bar is the time it takes the compressive wave to travel from the location of contact, reflect of the free end as a tensile wave, and then return to the location of contact. In other words, the time of contact is the time it takes a longitudinal wave to traverse the impactor twice which is $t = 2l/c$. From these assumptions, the impact can be modeled as a stress applied to the end of the bar over a finite length of time. The magnitude of the applied stress is 160 ksi and the duration is 2.5×10^{-6} seconds. The rise and drop times for the load wave are each 1.0e-07 seconds. This problem was simulated using the Tied-Node VFE approach described in this report. Figure 132 shows the results of this simulation at time 1.0e-04 seconds

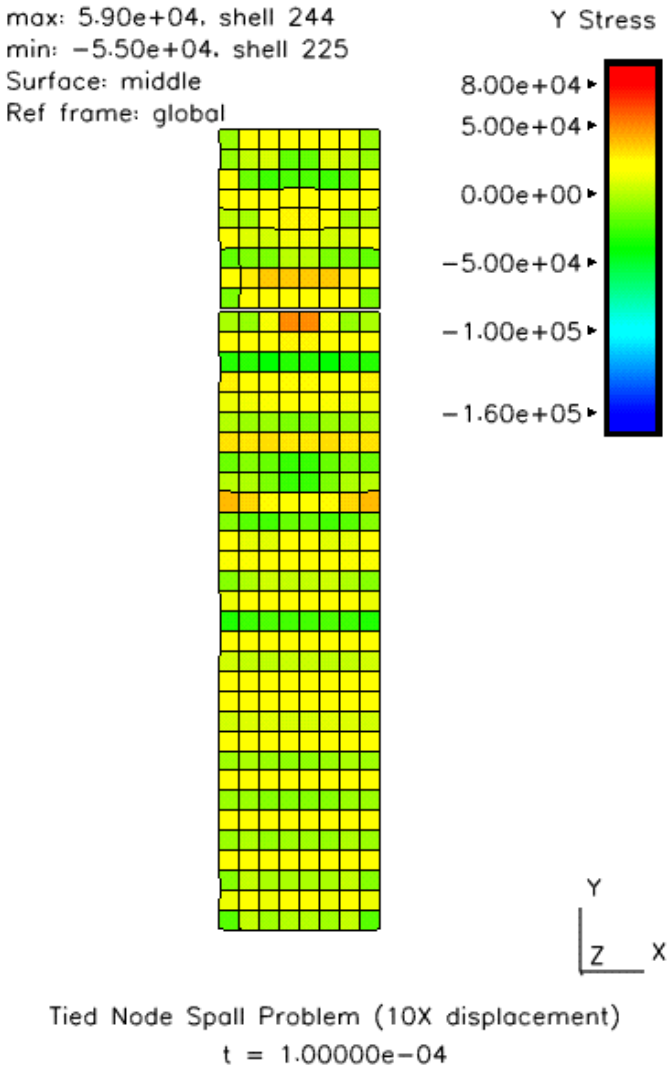

Figure 132. Tied Node Simulation of Impact Bar.

The simulation indicates that the ends spall off at 9.6875 in. from the impacted end. Spall at this location starts on the outer edges of the bar at 7.33e-5 seconds and propagates symmetrically inward to finish by 7.45e-5 seconds.

A Three Dimensional Tied-Node Implementation.

A Tied-Node VFE implementation has also been completed in DYNA3D using three-dimensional brick elements in a mult-noded three-dimensional mesh. Each face of each brick can accommodate a crack at the interface modeled as described in this report or other kinds of interface failure models can be encorporated. As an initial test of this approach simulation of the impact of the bar shown in Figure 131 was undertaken using

the 3D Tied-Node DYNA3D discrete fracture model. In this initial simulation, no fracture mechanics was encorporated into the model, however, and the surface separation was taken to occur when a critical stress level was achieved. Hot Link 133 presents the results of this three dimensional simulation in the form of a movie at 3dspall.501.mov .

A significant amount of progress has been demonstrated toward the goal of having robust verified and validated codes that can simulate the wave propagation and fragmentation of structures. Further work is needed to improve the fidelity of these codes. Such work continues.

ACKNOWLEGEMENT

The financial support of the Los Alamos National Laboratory under contract Number I1473-0019-23 to Colorado State University is gratefully acknowledged. The technical vision, guidance and encouragement of Dr. J. G. Bennett have been invaluable and without his participation, it would not have been possible to achieve this work. The creative and insightful work of Mr. Jobie Gerken on implementing and debugging the codes for this work has been outstanding and immeasurably valuable.

REFERENCES

1. Li, Z., Reed, M., 1995, "A Finite Element Method to Model Progressive Fracture," *Computer Methods in Applied Mechanics and Engineering,* Vol. 120, pp. 303-313.

2. Goodman, R. E., Taylor, R. L., Brekke, T. L., 1968 " A Model for the Mechanics of Jointed Rock," *Proceedings of the ASCE: Journal of the Soil Mechanics and Foundations Division*, Vol. 98, pp. 637-659.

3. M. Kanninen, J. Brust, J. Ahmad, and I. Abou-Sayed, "The Numerical Simulation of Crack Growth in Weld-Induced Residual Stress Fields", *Residual Stress and Stress Rela*xation, Ed. E. Kula and V. Weiss, Plenum Press, New York, 1982.

4. B. Liaw, A. S. Kobayashi, A. F. Emery, "Double Noding Technique for Mixed Mode Crack Propagation Studies", *International Journal for Numerical Methods in Engineering*, Vol. 20, pp 967-977, 1984.

5. Needleman, A., 1987, "A Continuum Model for Void Nucleation by Inclusion Debonding," *Journal of Applied Mechanics,* Vol. 54, pp. 525-531.

6. Needleman, A., 1992, "Micromechanical Modelling of Interfacial Decohesion," *Ultramicroscopy,* Vol. 40, pp. 203-214.

7. Xu, X. P., Needleman, A., 1993, "Void Nucleation by Inclusion Debonding in a Crystal Matrix," *Modelling and Simulation in Materials Science and Engineering,* Vol. 1, pp. 111-132.

8. Xu, X. P., Needleman, A., 1994a, "Erratum; Void Nucleation by Inclusion Debonding in a Crystal Matrix," *Modelling and Simulation in Materials Science and Engineering,* Vol. 2, pp. 417-418.

9. Xu, X. P., Needleman, A., 1994b, "Numerical Simulations of Fast Crack Growth in Brittle Solids," *Journal of the Mechanics and Physics of Solids,* Vol. 42, pp. 1397-1434.

10. Needleman, A., 1997, "Numerical Modeling of Crack Growth Under Dynamic Loading Conditions," *Computational Mechanics,* Vol. 19, pp. 463-469.

11. Siegmund, T., Needleman, A., 1997, "A Numerical Study of Dynamic Crack Growth in Elastic-Viscoplastic Solids," *International Journal of Solids and Structures,* Vol. 7, pp. 769-787.

12. Siegmund, T., Fleck, N. A., Needleman, A., 1997, "Dynamic Crack Growth Across an Interface," *International Journal of Fracture,* Vol. 85, pp. 381-402.

13. Camacho, G. T., Ortiz, M., 1996, "Computational Modeling of Impact Damage in Brittle Materials," *International Journal of Solids and Structures*, Vol. 33, pp. 2899-2938.

14. Xu, X. P., Needleman, A, Abraham, F. F., 1997, "Effect of Inhomogeneities on Dynamic Crack Growth in an Elastic Solid," *Modelling and Simulation in Materials Science and Engineering,* Vol. 5, pp. 489-516.

15. Potapov, A. V., Hopkins, M. A., Campbell, C. S., 1995a, "A Two – Dimensional Dynamic Simulation of Solid Fracture, Parts I & II", *International Journal of Modern Physics C*, Vol. 6, pp. 371-425.

16. Potapov, A. V., Campbell, C. S., 1996, "A Hybrid Finite – Element Simulation of Solid Fracture," *International Journal of Modern Physics C*, Vol. 7, pp. 155-180.

17. Potapov, A. V., Campbell, C. S., 1996, "A Three – Dimensional Simulation of Brittle Solid Fracture," *International Journal of Modern Physics C*, Vol. 7, pp. 717-729.

18. Belytschko, T., Lu, Y. Y., Gu, L., 1995, "Crack Propagation by Element-Free Galerkin Methods," *Engineering Fracture Mechanics,* Vol. 51, pp. 295-315.

19. Belytschko, T., Lu, Y. Y., Gu, Y., Tabbara, M., 1995, "Element-Free Galerkin Methods for Static and Dynamic Fracture," *International Journal of Solids and Structures,* Vol. 32, pp. 2547-2570.

20. Belytschko, T., Organ, D., Krongauz, Y., 1995 "A Coupled Finite Element – Element-Free Galerkin Method," *Computational Mechanics,* Vol. 17, pp. 186-195.

21. Belytschko, T., Tabbara, M., 1996, "Dynamic Fracture using Element-Free Galerkin Methods," *International Journal for Numerical Methods in Engineering,* Vol. 39, pp. 923-938.

22. Sukumar, N., Moran, B., Black, T., Belytschko, T., 1997, "An Element-Free Galerkin Method for Three-Dimensional Fracture Mechanics," *Computational Mechanics,* Vol. 20, pp. 170-175.

23. Fleming, M., Chu, Y. A., Moran, B., Belytschko, T., 1997, "Enriched Element-Free Galerkin Methods for Crack Tip Fields," *International Journal for Numerical Methods in Engineering,* Vol. 40, pp. 1483-1504.

24. Hertzberg, R. W., Deformation and Fracture Mechanics of Engineering Materials, John Wiley and Sons, 4th Ed., 1995.

25. Gerken, J.M., *An Implicit Finite Element Method for Discrete Dynamic Fracture*, MS Thesis, Colorado State University, 1998.

26. Stout, M. G.; Liu, C., MST-8, Los Alamos National Laboratory, Personal Communication, 1998.

27. Crane L. W. and Bigg, A. P., "Fracture Toughness of High Speed Steels", *Material Science and Technology*, October, 1990, vol. 6, pp 993 – 998.